A model for fluvial bedrock incision by impacting suspended and bed load sediment

Michael P. Lamb,[1] William E. Dietrich,[1] and Leonard S. Sklar[2]

[1] A mechanistic model is derived for the rate of fluvial erosion into bedrock by abrasion from uniform size particles that impact the bed during transport in both bed and suspended load. The erosion rate is equated to the product of the impact rate, the mass loss per particle impact, and a bed coverage term. Unlike previous models that consider only bed load, the impact rate is not assumed to tend to zero as the shear velocity approaches the threshold for suspension. Instead, a given sediment supply is distributed between the bed and suspended load by using formulas for the bed load layer height, bed load velocity, logarithmic fluid velocity profile, and Rouse sediment concentration profile. It is proposed that the impact rate scales linearly with the product of the near-bed sediment concentration and the impact velocity and that particles impact the bed because of gravitational settling and advection by turbulent eddies. Results suggest, unlike models that consider only bed load, that the erosion rate increases with increasing transport stage (for a given relative sediment supply), even for transport stages that exceed the onset of suspension. In addition, erosion can occur if the supply of sediment exceeds the bed load transport capacity because a portion of the sediment load is transported in suspension. These results have implications for predicting erosion rates and channel morphology, especially in rivers with fine sediment, steep channel-bed slopes, and large flood events.

Citation: Lamb, M. P., W. E. Dietrich, and L. S. Sklar (2008), A model for fluvial bedrock incision by impacting suspended and bed load sediment, *J. Geophys. Res.*, *113*, F03025, doi:10.1029/2007JF000915.

1. Introduction

[2] River incision into bedrock is one of the fundamental drivers of landscape evolution and propagates climatic and tectonic signals throughout drainage networks. Incision into rock occurs relatively slowly and during large infrequent events making it difficult to investigate mechanistically. To characterize river incision geomorphologists typically have relied on reach-scale rules, for example, by setting the rate of erosion to be a function of boundary shear stress [*Howard and Kerby*, 1983] or stream power [*Seidl and Dietrich*, 1992; *Howard et al.*, 1994; *Seidl et al.*, 1994; *Whipple and Tucker*, 1999]. These models are limited in application, however, because they mask the physical mechanisms by which bedrock erosion occurs. More realistic model predictions require advances in our quantitative understanding of erosion processes [e.g., *Dietrich et al.*, 2003; *Whipple*, 2004].

[3] One such model proposed by *Sklar and Dietrich* [2004] explicitly models the wear of bedrock by bed load particles (referred to as the saltation-abrasion model herein). Application of the saltation-abrasion model and related

efforts have led to significant insights into the controls of bedrock river morphology including, channel slope [*Sklar and Dietrich*, 2006; *Gasparini et al.*, 2007], knickpoints [e.g., *Chatanantavet and Parker*, 2005; *Wobus et al.*, 2006; *Crosby et al.*, 2007], slot canyons [*Carter and Anderson*, 2006; *Johnson and Whipple*, 2007], and channel width [*Finnegan et al.*, 2007; *Nelson and Seminara*, 2007; *Turowski et al.*, 2008]. Nonetheless, the saltation-abrasion model is incomplete because it neglects other important mechanisms for riverbed erosion such as cavitation, plucking of jointed rock and abrasion by suspended sediment [*Whipple et al.*, 2000]. Abrasion by suspended sediment in particular has been argued to be an important or dominant erosion mechanism in some streams [*Hancock et al.*, 1998; *Whipple et al.*, 2000; *Hartshorn et al.*, 2002] owing in part to the frequent occurrence of polished bedrock surfaces, flutes, potholes, and undulating canyon walls.

[4] In this paper, we investigate erosion by suspended particles by deriving a total load erosion model, which expands on the saltation-abrasion model of *Sklar and Dietrich* [2004] to include suspended particles. Cavitation and plucking of jointed rock are not investigated here. In section 2, the saltation-abrasion model is reviewed briefly and the assumption that the impact rate is zero at the onset of suspension is discussed. In section 3, we propose that suspended particles do interact with the bed and that the impact rate scales with the product of the near-bed sediment concentration and the particle impact velocity. The near-bed

[1]Department of Earth and Planetary Science, University of California, Berkeley, California, USA.
[2]Department of Geosciences, San Francisco State University, San Francisco, California, USA.

sediment concentration is found by partitioning a given sediment supply between the bed and suspended load. In section 4, commonly used formulas are adopted to solve the model, including the Rouse concentration profile to describe the vertical distribution of suspended sediment. In section 5, predictions of the total load erosion model are shown and compared to the saltation-abrasion model for different values of transport stage, sediment supply, particle size, and channel slope. Finally, the entrainment capacity, viscous damping of impacts, and implications for natural streams are discussed in section 6.

2. Saltation-Abrasion Model

[5] *Sklar and Dietrich* [2004], following the work of *Foley* [1980], *Beaumont et al.* [1992], *Tucker and Slingerland* [1994], and others, present a model for fluvial incision of bedrock by saltating sediment, which is briefly reviewed here. The saltation-abrasion model was formulated by neglecting abrasion by all modes of sediment transport except saltation. A planar bed, rectangular channel cross section, and uniform size sediment are assumed. The model assumes that the net effects of spatial heterogeneity in hydraulics, rock strength, and sediment supply can be adequately represented in terms of a unit bed area.

[6] The rate of vertical erosion E is defined as the product of the average volume of rock detached per particle-bedrock impact V_i, the rate of particle impacts per unit bed area per unit time I_r, and the fraction of exposed bedrock on the river bed F_e

$$E = V_i I_r F_e. \tag{1}$$

The volume of eroded bedrock per particle impact V_i is scaled by the kinetic energy of the particle impact

$$V_i = \frac{1}{2} \frac{V_p \rho_s w_i^2}{\varepsilon_v}, \tag{2}$$

where V_p, ρ_s, and w_i are the particle volume, density, and impact velocity normal to the bed. A threshold kinetic energy needed to cause erosion is not included on the basis of results from abrasion mill experiments [*Sklar and Dietrich*, 2001]. The kinetic energy required to cause erosion of a unit volume of bedrock ε_v (units of energy per volume) depends on the capacity of the rock to store energy elastically

$$\varepsilon_v = k_v \frac{\sigma_T^2}{2Y}, \tag{3}$$

where σ_T is the tensile yield strength and Y is Young's modulus of elasticity of the bedrock. The dimensionless coefficient k_v was found to be of the order 10^6 [*Sklar and Dietrich*, 2006].

[7] The rate of particle-bedrock impacts per unit bed area I_r is given by

$$I_r = \frac{q_b}{V_p L_b}, \tag{4}$$

where q_b is the volumetric sediment flux per unit channel width traveling as bed load and L_b is the saltation hop length. Note that q_b in this paper is the same as q_b/ρ_s defined by *Sklar and Dietrich* [2004], since they defined q_b to be a mass flux rather than a volumetric flux.

[8] Following the hypothesis of *Gilbert* [1877], the fraction of the river bed that is exposed bedrock and not covered with alluvium F_e is assumed to vary as

$$F_e = \left(1 - \frac{q_b}{q_{bc}}\right), \tag{5}$$

where q_{bc} is the volumetric bed load sediment transport capacity per unit channel width [*Sklar et al.*, 1996; *Slingerland et al.*, 1997; *Sklar and Dietrich*, 2004]. This linear relationship has yet to be tested in nature, and others have argued that an exponential relationship is more appropriate [*Turowski et al.*, 2007]. Herein we use equation (5) to simplify later comparison of the saltation-abrasion model with the total load erosion model. Equation (5) must be true in end-member cases at steady state. Where the supply of sediment exceeds the transport capacity, sediment is deposited on the bed and the bedrock is protected from erosion. This is typically the case in alluvial, transport-limited rivers and many formulas exist to predict the sediment transport (and hence the transport capacity) under such conditions [e.g., *Fernandez Luque and van Beek*, 1976]. On the other hand, if the sediment supply is zero, the river bed will be free of cover. In this case, however, no erosion will occur because there are no particles to impact the bed.

[9] Combining equations (1)–(5) yields the composite expression of the saltation-abrasion model

$$E = \frac{\rho_s q_b w_i^2 Y}{L_b k_v \sigma_T^2} \left(1 - \frac{q_b}{q_{bc}}\right). \tag{6}$$

[10] Most important for the present study is evaluation of the saltation hop length L_b. *Sklar and Dietrich* [2004] compiled data from numerous experimental and theoretical studies on particle saltation [*Francis*, 1973; *Abbott and Francis*, 1977; *Wiberg and Smith*, 1985; *Sekine and Kikkawa*, 1992; *Lee and Hsu*, 1994; *Nino et al.*, 1994; *Hu and Hui*, 1996] and found the best fit relationship to be

$$\frac{L_b}{D} = 8.0 \left(\frac{\tau_*}{\tau_{*c}} - 1\right)^{0.88}, \tag{7}$$

where D is the particle diameter and τ_*/τ_{*c} is the transport stage. The nondimensional bed stress or Shields stress is given by

$$\tau_* = \frac{u_*^2}{RgD}, \tag{8}$$

where $R = (\rho_s - \rho_f)/\rho_f$ is the submerged specific density of the sediment, ρ_f is the density of the fluid, g is the acceleration due to gravity, and u_* is the bed shear velocity. The critical value of the Shields stress (τ_{*c}) is the value of τ_* at the threshold of particle motion [*Shields*, 1936].

[11] In the saltation-abrasion model, particle-hop length is assumed to be infinite for particles transported in suspension. A flow is typically considered competent to suspend sediment if

$$u_*/w_{st} \geq 1, \tag{9}$$

where w_{st} is the terminal settling velocity of the sediment [*Bagnold*, 1966]. Therefore, *Sklar and Dietrich* [2004] modified equation (7) to be

$$\frac{L_b}{D} = \frac{8.0(\tau_*/\tau_{*_c} - 1)^{0.88}}{\sqrt{1 - (u_*/w_{st})^2}} \quad (10)$$

and the erosion rate (equation (6)) is zero if $u_*/w_{st} \geq 1$.

[12] The experimental particle trajectory data used to calibrate equation (10) does not extend into the regime $u_*/w_{st} \geq 1$, and thus the validity of equation (10) over equation (7) cannot be verified. We hypothesize that suspended sediment does contribute to bedrock erosion due to particle-bedrock impacts. In the next section, we develop this hypothesis and present a model for bedrock erosion from suspended and bed load sediment.

3. Total Load Erosion Model

[13] Our model development follows the assumptions and limitations of previous work on erosion by bed load discussed above. In particular, our model considers incision into a flat bed of unit area by impacts of single sized particles. The model is based on the concept that suspended sediment actually is not held in a fluid indefinitely. Instead, particles are continuously falling through the fluid due to gravitational settling and are advected toward the bed due to turbulence. Where $u_*/w_{st} \geq 1$, sediment travels both in suspension and bed load [*Bagnold*, 1966; *van Rijn*, 1984; *Nino et al.*, 2003]. Therefore, the incision model is developed to include impacts by both bed load and suspended particles (i.e., the total load) under a wide range of conditions including $u_*/w_{st} \geq 1$.

3.1. Settling Flux

[14] During conditions of suspended sediment transport (i.e., $u_*/w_{st} \geq 1$), particles do impact and interchange with the bed. Particles are entrained from the bed by coherent flow structures, which produce bursts of upward moving fluid [*Grass*, 1970; *Jackson*, 1976; *Sumer and Deigaard*, 1981; *Nelson et al.*, 1995; *Bennett et al.*, 1998]. As these structures dissipate, particles tend to settle toward the bed at a rate near their settling velocity in still water [e.g., *Sumer and Deigaard*, 1981; *Ninto and Garcia*, 1996]. This gravitational settling results in a volumetric flux per unit area of sediment toward the bed given by

$$f_s = c_b w_s, \quad (11)$$

where c_b is the near-bed volumetric sediment concentration and w_s is the gravitational settling velocity of the sediment (which can be less than w_{st}). Despite this downward sediment flux, an equilibrium concentration of particles can be attained because there is a dynamic balance between the upward and downward fluxes of particles [*Rouse*, 1937; *Smith and McLean*, 1977; *Parker*, 1978; *García and Parker*, 1991; *Bennett et al.*, 1998].

[15] This concept is well illustrated in the experiments of *Einstein* [1968] in which a recirculating flume was used to create a steady, uniform flow over an open framework and immobile gravel bed. The flow was highly turbulent and capable of suspending the silt that was introduced into the flume (u_*/w_{st} ranged from 74 to 7.2×10^3). Despite the fact that $u_*/w_{st} \gg 1$, the *suspended* particles did indeed impact the bed, as the turbid flows eventually clarified, and a steady state concentration profile was not attained. This was because the suspended silt settled through the gravel on the flume bed and the downward flux of sediment was not balanced by a commensurate entrainment flux from the bed.

3.2. Particle-Bed Impacts

[16] Few experimental studies have traced the flow paths of individual suspended particles, which, along with the stochastic nature of such trajectories, makes it difficult to directly formulate an effective particle hop length for suspension. Since classic suspension theory is based in terms of sediment concentration [*Rouse*, 1937], it is useful to formulate the impact rate as a function of sediment concentration instead of hop length. Following the above arguments and equation (11), the rate of particle impacts per unit bed area can be expected on average to be proportional to the product of the near-bed sediment concentration and the particle velocity normal to the bed,

$$I_r = \frac{A_1 c_b w_i}{V_p}. \quad (12)$$

The impact velocity normal to the bed (w_i) is used here as a measure of the particle velocity instead of the gravitational settling velocity (w_s, as in equation (11)) because w_s might not be normal to the bed and impacts also can occur because of turbulent fluctuations (discussed in section 4.4). The coefficient $A_1 < 1$ accounts for the fact that some of the particles near the bed are advected upward because of lift forces.

[17] Equation (12) is not specific to suspension and also holds for bed load. For example, the downstream flux of bed load sediment can be written as

$$q_b = c_b U_b H_b, \quad (13)$$

where U_b is the vertically averaged stream-wise particle velocity and c_b is the vertically averaged sediment concentration within the bed load layer of height H_b. The average bed load velocity can be scaled as

$$U_b = \frac{L_b}{t_i} \approx \frac{A_2 w_s L_b}{H_b}, \quad (14)$$

where t_i is the timescale between bed impacts for an individual particle. $A_2 < 1$ accounts for the fact that the average fall velocity within the bed load layer might be less than the near-bed settling velocity, and that the total time between impacts should also include the particle ejection or risetime as well as the fall time. For example, *Sklar and Dietrich* [2004] suggest $A_2 \approx 1/3$. Combination of equations (4), (13), and (14) results in

$$I_r = \frac{A_2 c_b w_s}{V_p}, \quad (15)$$

which is the same as equation (12) provided that $A_2 w_s = A_1 w_i$.

3.3. Sediment Supply

[18] In alluvial rivers with an unlimited supply of sediment on the bed and a steady state concentration profile, the settling flux of sediment near the bed f_s is equal to the entrainment capacity of the flow (per unit bed area) F_e, which can be written as

$$f_e = \alpha w_s, \tag{16}$$

where α is a nondimensional sediment entrainment parameter (which is a function of u_*/w_{st} [e.g., *García and Parker*, 1991]). Thus, where $f_e = f_s$, the near bed sediment concentration c_b can be determined directly from the hydraulics and sediment size because combination of equations (11) and (16) results in $\alpha = c_b$. This is not the case in bedrock rivers.

[19] For supply limited conditions typical of bedrock rivers, the concentration of particles in suspension (and therefore c_b) is not dependent on the entrainment capacity (i.e., $\alpha > c_b$) and instead is determined by the sediment supply from the bed, banks, and upstream. By continuity

$$q_s = \int_{H_b}^{H} cudz = c_b UH\chi, \tag{17}$$

where q_s is the volumetric flux of sediment per unit channel width traveling in suspension, c and u are the depth-dependent concentration and downstream flow velocity per unit channel width averaged over turbulent fluctuations, U is the depth-averaged flow velocity in the downstream direction, H is the flow depth, z is the coordinate perpendicular to the river bed, and $0 \leq \chi \leq 1$ is the integral that describes the vertical structure of velocity and concentration. In equation (17), it is assumed that the average stream-wise particle velocities are equal to the fluid velocities, as is typical for suspended sediment [e.g., *McLean*, 1992].

[20] To evaluate the impact rate given by equation (12), the near-bed sediment concentration must be known. Here, we seek an expression for the near-bed concentration by partitioning the supplied sediment flux into bed and suspended load. To simplify matching the concentration profile between the bed load and the suspended sediment above, we assume that within the bed load layer ($z \leq H_b$) sediment is well mixed [e.g., *McLean*, 1992] with a concentration of c_b (Figure 1). Equations (13) and (17) can be summed and solved for c_b as

$$c_b = \frac{q}{UH\chi + U_b H_b}, \tag{18}$$

where q is the total volumetric flux of sediment traveling as both bed and suspended load per unit width, which is equivalent to the total sediment supply (per unit width) in the supply limited conditions considered here. Thus, inclusion of suspended sediment (rather than considering only bed load) reduces the near-bed sediment concentration and therefore the rate of impacts for a given sediment supply. Equation (18), however, predicts a finite near-bed sediment concentration for all flow conditions.
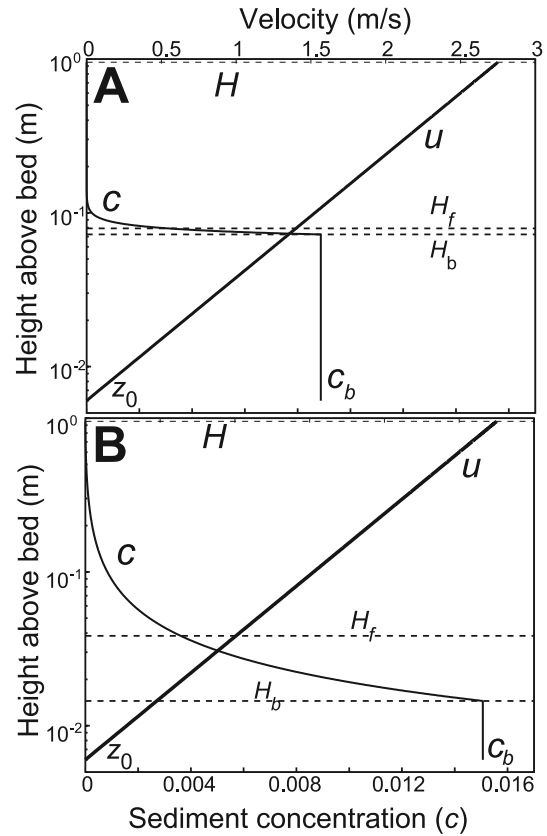
Figure 1. Schematic showing vertical profiles of sediment concentration c (equation (26)) and velocity u (equation (21)) for the conditions of the Eel River (Table 1) and for (a) 60-mm gravel and (b) 1-mm sand. Also shown are the calculated heights of the bed load layer H_b (equation (25)), weighted average particle fall heights H_f (equation (32)), flow depth H (Table 1), and the near-bed sediment concentration c_b (equation (18)).

3.4. Composite Expression for the Total Load Erosion Model

[21] Substituting equations (2), (3), (5), (12), and (18) into equation (1) yields the combined model for erosion by bed and suspended sediment

$$E = \frac{A_1 \rho_s Y}{k_v \sigma_T^2} \frac{q w_i^3}{(UH\chi + U_b H_b)} \left(1 - \frac{q_b}{q_{bc}}\right), \tag{19}$$

where q_b is found from equations (13) and (18) to be

$$q_b = q\left(\frac{U_b H_b}{UH\chi + U_b H_b}\right). \tag{20}$$

4. Empirical Expressions and Calculation Procedure

[22] Following *Sklar and Dietrich* [2004], the total load erosion model is explored here by holding some variables to constant values typical of a reference field site, the South

Table 1. Model Input and Output Values for Representative Field Case: South Fork Eel River, California

Parameter	Value
Channel slope, S	0.0053
Channel width, W	18 m
Sediment supply, q_s	8.9×10^{-4} m^2/s
Water discharge, q_w	2.1 m^2/s
Flow velocity, U	2.2 m/s
Flow depth, H	0.95 m
Shear velocity, u_*	0.22 m/s
Rock tensile strength, σ_T	7 MPa
Young's elastic modulus, Y	5.0×10^4 MPa
Rock resistance parameter, k_v	1.0×10^6
Critical Shields stress, τ_{*c}	0.03
Sediment density, ρ_s	2650 kg/m^3
Water density, ρ_f	1000 kg/m^3
Kinematic viscosity of water, ν	10^{-6} m^2/s
Sediment size, D	60 mm, 1 mm
Transport stage, τ_*/τ_{*c}	1.7, 102
Particle fall height, H_f	79 mm, 38 mm
Terminal settling velocity, w_{st}	0.98 m/s, 0.13 m/s
Bed load velocity, U_b	1.26 m/s, 2.2 m/s
Bed load concentration, c_b	0.0089, 0.0151
Bed load layer height, H_b	72.3 mm, 14.5 mm
Bed load transport capacity, q_{bc}	1.0×10^{-3} m^2/s, 3.8×10^{-3} m^2/s
Erosion rate, E	31 mm/a, 10 mm/a

Fork Eel River, California, USA [*Seidl and Dietrich*, 1992; *Howard*, 1998]. As shown in Table 1, the characteristic sediment size and supply is set to $D = 60$ mm and $q = 8.9 \times 10^{-4}$ m^3/s (see *Sklar* [2003] for details) on the basis of the average landscape lowering rate of 0.9 mm/a (where a is years) [*Merritts and Bull*, 1989]. The representative discharge is 39.1 m^3/s, which has an exceedence probability of 0.013 and a transport stage of $\tau_*/\tau_{*c} = 1.7$ [*Sklar and Dietrich*, 2004]. Given this transport stage, the representative flow depth is found to be $H = 0.95$ m assuming $\tau_{*c} = 0.03$ (Table 1).

[23] To better show the effects of suspension, we also consider 1-mm sand in addition to the 60-mm gravel. Note that our model is formulated in terms of single sized particles that travel in both suspended load and bed load. A model incorporating multiple particle sizes interacting and impacting the bed at the same time is not attempted here. Thus, the following calculations assume that the total load is composed either exclusively of 60-mm gravel or exclusively 1-mm sand. For the later case, the hydraulic and geometric conditions are set to the same representative values used for $D = 60$ mm for purposes of comparison. In particular, with an equivalent representative discharge and flow depth, the transport stage for the 1-mm sand is found to be $\tau_*/\tau_{*c} = 102$ (Table 1). For simplicity, we use a constant value of $\tau_{*c} = 0.03$ throughout, although a particle Reynolds number or relative roughness dependency could be explored in the future [*Buffington and Montgomery*, 1997; *Lamb et al.*, 2008].

[24] To solve equation (19), expressions for the flow velocity, bed load transport capacity, bed load layer height and velocity, sediment concentration, and impact velocity are needed. Relatively simple and commonly used formulas for these variables are employed here.

4.1. Flow Velocity

[25] For turbulent boundary layer flow in a channel, the downstream velocity can be calculated as

$$u = \frac{u_*}{\kappa} \ln\left(\frac{z}{z_0}\right), \tag{21}$$

where z_0 is a function of the boundary roughness and κ is von Karman's constant ($\sim$0.41) (Figure 1). The shear velocity is calculated from $u_* = (gH \sin\theta)^{1/2}$, where θ is the channel-bed slope angle. Strictly speaking, equation (21) is only applicable to the lower $\sim$20% of the water column, and an adjustment to the eddy viscosity could be made for the upper portion of the flow [e.g., *Coles*, 1956; *Gelfenbaum and Smith*, 1986]. Modifications to the eddy viscosity could also be made because of stratification and form roughness [*Vanoni*, 1946; *McLean*, 1992; *Wright and Parker*, 2004]. For simplicity we assume that equation (21) is applicable throughout the water column and integrate to find the depth-averaged flow velocity

$$U = \frac{1}{H}\int_{z_0}^{H} \frac{u_*}{\kappa} \ln\left(\frac{z}{z_0}\right) dz. \tag{22}$$

For the following calculations we set $z_0 = nD/30$ with the empirical coefficient $n = 3$ [e.g., *Kamphius*, 1974]. To hold the hydraulic conditions constant for $D = 60$ mm and $D = 1$ mm, we evaluate the roughness using $D = 60$ mm for both cases. This is done to simplify comparison. We suspect, however, that this might be an inaccurate parameterization of the hydraulic roughness in natural bedrock streams where the bed is only partially covered with sediment. Furthermore, roughness might be dominated by the banks, immobile boulders, or sculpted forms on the bed [*Finnegan et al.*, 2007; *Johnson and Whipple*, 2007; *Yager et al.*, 2007].

[26] The resulting velocity profile for the representative conditions of the South Fork Eel River using equation (21) are shown in Figure 1. The depth-averaged velocity is calculated from equation (22) to be $U = 2.2$ m/s (Table 1).

4.2. Bed Load Transport Capacity, Layer Height, Concentration, and Velocity

[27] Many equations exist for the bed load transport capacity. Here, we use the relation of *Fernandez Luque and van Beek* [1976]:

$$q_{bc} = 5.7\left(RgD^3\right)^{1/2}\left(\tau_* - \tau_{*c}\right)^{3/2}. \tag{23}$$

The sediment transport capacity for the two representative cases is found to be 1.0×10^{-3} m^2/s and 3.8×10^{-3} m^2/s for the 60-mm gravel and the 1-mm sand, respectively (Table 1).

[28] The depth-averaged bed load velocity and layer height are given as empirical expressions by *Sklar and Dietrich* [2004] derived from several different bed load studies. The best fit relationships are

$$U_b = 1.56(RgD)^{1/2}\left(\frac{\tau_*}{\tau_{*c}} - 1\right)^{0.56} \tag{24}$$

and

$$H_b = 1.44 D \left(\frac{\tau_*}{\tau_{*c}} - 1 \right)^{0.50}. \qquad (25)$$

The bed load velocities and layer heights for the two representative cases are found to be $U_b = 1.26$ m/s and $H_b = 72.3$ mm for the 60-mm gravel, and $U_b = 2.6$ m/s and $H_b = 14.5$ mm for the 1-mm sand (Table 1). For the sand, equation (24) predicts a bed load velocity that is greater than the depth averaged fluid velocity. The high transport stage for the sand ($\tau_*/\tau_{*c} = 102$) is beyond the range of empirical data used to formulate equation (24). At large transport stages, particle velocities instead approach the fluid velocity [e.g., *Bennett et al.*, 1998]. To account for this effect, we set $U_b = U$ where equation (24) predicts $U_b > U$. Likewise, in rare cases with large transport stages, large channel slopes, and small flow depths, the empirical equation (25) predicts a bed load layer height (i.e., a saltation hop height) that is greater than the flow depth. In reality, under these conditions the bed load layer likely occupies the entire depth of flow. Therefore, where this occurs we set $H_b = H$. Using these expressions, the near-bed concentration of particles (equation (18)) is found to be 0.0089 and 0.0151 for the 60-mm gravel and the 1-mm sand, respectively (Table 1).

4.3. Vertical Structure of Suspended Load

[29] To evaluate the erosion rate, the vertical structure of the suspended sediment load must be known. Here we use the most widely accepted expression for the vertical profile of suspended sediment, *Rouse*'s [1937] equation

$$c = c_b \left[\frac{(1 - \zeta_z)/\zeta_z}{(1 - \zeta_b)/\zeta_b} \right]^P, \qquad (26)$$

where $\zeta_z = z/H$, $\zeta_b = H_b/H$, and $P = w_{st}/\beta \kappa u_*$ is the Rouse parameter (Figure 1). To arrive at equation (26), Rouse balanced the entrainment and settling flux of suspended sediment, and scaled the entrainment flux as a diffusive process using a parabolic eddy viscosity profile for steady, uniform flow

$$\nu_T = \beta u_* \kappa z (1 - z/H). \qquad (27)$$

The coefficient β is typically thought to be a constant of order unity and accounts for any differences between the diffusivity of momentum and sediment.

[30] As discussed above for the logarithmic velocity profile, several authors have argued that the Rouse profile should not apply because equation (27) is only applicable to the lower 10–20% of the water column. Nonetheless, experimental data support use of the Rouse equation throughout the water column, with β ranging from approximately 0.5 to 3 [*Bennett et al.*, 1998; *Graf and Cellino*, 2002; *Nezu and Azuma*, 2004; *Wren et al.*, 2004; *Muste et al.*, 2005]. Because of the present uncertainty in the value of β, we assume that $\beta = 1$ in the following calculations.

[31] To apply equation (26), the near-bed concentration c_b is calculated from equation (18), where the integral relating

suspended sediment flux to the bulk parameters of the flow (χ) can be found from equations (17), (21), and (26) as

$$\chi = \frac{1}{UH} \int\limits_{H_b}^{H} \left[\frac{(1 - \zeta_z)/\zeta_z}{(1 - \zeta_b)/\zeta_b} \right]^{\frac{w_{st}}{\kappa u_*}} \frac{u_*}{\kappa} \ln\left(\frac{z}{z_0} \right) dz. \qquad (28)$$

The resulting concentration profiles for the representative cases are shown in Figure 1. Because of the low transport stage, most of the 60-mm gravel is contained within the bed load layer. In contrast, a significant portion of the sediment extends above H_b for the 1-mm sand.

4.4. Particle Impact Velocity

[32] For saltating sediment, *Sklar and Dietrich* [2004] used a scaling analysis combined with their empirical fits for L_b, U_b, and H_b to obtain an expression for the impact velocity,

$$w_i = 0.8(RgD)^{1/2} \left(\frac{\tau_*}{\tau_{*c}} - 1 \right)^{0.18} \left(1 - \left(\frac{u_*}{w_{st}} \right)^2 \right)^{1/2}. \qquad (29)$$

Equation (29) cannot be used in our model because the empirical data used to calibrate the equation does not extend into the suspension regime.

[33] As an alternative approach, we consider impacts at the bed due to gravitational settling of particles and advection by turbulent eddies. First, we calculate the impact velocity due to gravitational settling directly from a momentum balance for a falling particle. It is important to calculate the settling velocity as a function of fall distance because large particles might not have sufficient settling distance to reach terminal velocity upon impact. The component of the particle settling velocity normal to the bed can be calculated from a balance between the forces of gravity and drag as

$$w_s = w_{st} \cos\theta \sqrt{1 - \exp\left(-\frac{3 C_d \rho_f H_f}{2 \rho_s D \cos\theta} \right)}, \qquad (30)$$

where

$$w_{st} = \left(\frac{4}{3} \frac{RgD}{C_d} \right)^{1/2} \qquad (31)$$

is the terminal settling velocity (see Appendix A). The drag coefficient C_d depends on the particle Reynolds number and grain shape, and we calculate C_d from the empirical formula of *Dietrich* [1982] for natural sediment (Corey shape factor = 0.8, Powers roundness scale = 3.5).

[34] The particle velocity given by equation (30) depends on the distance over which a particle falls (H_f). In a combined bed load and suspension flow, particles are falling from all distances above the bed (z), from the top of the bed load layer to the depth of the flow ($H_b \leq z \leq H$). For uniform-size sediment, the average height from which particles fall should depend on the fraction of particles that are suspended to that elevation. Therefore, the shape of the steady state concentration profile should reflect the relative

heights that particles are suspended (and therefore their fall distances). To incorporate these effects, we propose an average fall distance that is weighted by the proportion of the total near-bed sediment c_b that is suspended to that height,

$$H_f = \frac{1}{c_b} \int\limits_H^{H_b} z \frac{dc}{dz} dz. \tag{32}$$

If all sediment is bed load, equation (32) predicts, as expected, that all particles fall from the top of the bed load layer (i.e., $H_f = H_b$) because we assume that sediment is uniformly mixed within the bed load layer (i.e., $\frac{dc}{dz} = 0$ for $z < H_b$). For 60-mm gravel, $H_f = 79.2$ mm, which is only slightly greater than the bed load layer height ($H_b = 72.3$ mm) (Figure 1). For 1-mm sand, $H_f = 38.4$ mm and is greater than $H_b = 14.5$ mm, because the high transport stage for the sand results in more of the load carried above H_b.

[35] In addition to gravitational setting of particles, turbulent fluctuations can affect the average particle-bed impact rate by advecting particles both away from the bed (reducing the impact rate) and toward the bed (increasing the impact rate). Rigorously characterizing the temporal and spatial variability in turbulent fluctuations is beyond the scope of this paper. As a first-order approach, we assume that turbulent fluctuations follow a Gaussian distribution [e.g., *Bridge and Bennett*, 1992; *Nezu and Nakagawa*, 1993; *Cheng and Chiew*, 1999]. The probability density function (P) of velocity fluctuations (w') is given by

$$P(w') = \frac{1}{\sqrt{2\pi}\sigma_w} \exp\left(-\frac{(w')^2}{2\sigma_w^2}\right), \tag{33}$$

where $\sigma_w = \sqrt{\overline{w'^2}}$ is the standard deviation of velocity fluctuations perpendicular to the bed and the overbar denotes a time average. The standard deviation of these velocity fluctuations has been shown to be approximately equal to u_* in open channel flow [*Nezu and Nakagawa*, 1993], which we employ here (i.e., $\sigma_w = u_*$).

[36] To calculate the particle impact velocity, we assume that particles follow the fluid, so that equation (33) can be used to calculate the probability of fluctuations in *particle* velocity, as well as fluid velocity. Furthermore, we assume that inertial forces dominate near the bed so that particles impact the bed and are not swept laterally with the flow (see section 6 for discussion). With these assumptions, the average impact velocity can be found by summing the component of the gravitational settling velocity perpendicular to the bed with the turbulent velocity fluctuations (which by definition are perpendicular to the bed), and integrating over all possible values of fluctuations as

$$w_i = \int\limits_{-w_s}^{6\sigma_w} (w' + w_s)P dw'. \tag{34}$$

The upper limit of integration was chosen because it incorporates very near 100% of the positive fluctuations (Figure 2). The lower limit defines the condition $w' + w_s = 0$; where $w' + w_s < 0$, particles are moving upward and the impact velocity and impact rate are zero. Thus, despite the fact that the Gaussian distribution is symmetrical, the mean
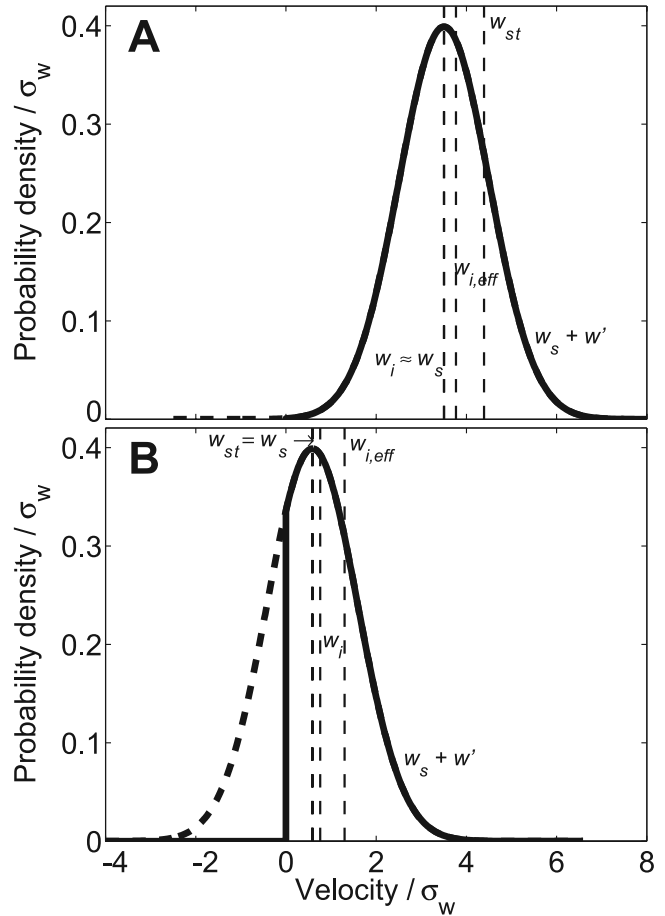
Figure 2. Probability density function for the particle velocity normalized by one standard deviation for (a) 60-mm gravel and (b) 1-mm sand. The density functions are centered about the gravitational settling velocity (w_s) and the distribution in velocity is due to turbulent fluctuations given by equation (33). The solid thick line shows the portion of the distribution that is integrated to calculate the average impact velocity (w_i) and the effective impact velocity ($w_{i,\mathrm{eff}}$). The dashed thick line is the portion of the distribution that is not included in the integration because only positive velocities produce impacts.

impact velocity can deviate from the gravitational settling velocity because the impact velocity must be nonnegative (Figure 2).

[37] The deviation of the impact velocity from the gravitational settling velocity is more important when considering that the erosion rate scales with the impact velocity cubed (equation (19)). The erosion rate depends on the cube of individual particle velocities (i.e., $w' + w_s$), however, and not the average impact velocity w_i. Thus to formulate an average impact velocity that scales with the erosion rate, we define the effective impact velocity by nonlinear averaging, as

$$w_{i,\mathrm{eff}} = \left[\int\limits_{-w_s}^{6\sigma_w} (w' + w_s)^3 P dw' \right]^{1/3}. \tag{35}$$

Similar to the turbulent fluctuations, the gravitational settling velocity also could be weighted to account for the cubic dependence of erosion rate on impact velocity, rather than using the velocity for the linearly averaged fall distance calculated in equation (32). We found, however, that accounting for this has a negligible effect on the results.

[38] For the gravel at $\tau_*/\tau_{*c} = 1.7$, the gravitational fall velocity is sufficiently large compared to the turbulent fluctuations, so that only the very tail of the distribution is within the regime $w' + w_s < 0$ (shown as a thick dashed line in Figure 2a). The result is that turbulent fluctuations tend to cancel, and therefore $w_i \approx w_s$. This notwithstanding, the minor asymmetry in the probability density function results in an average impact velocity that is slightly greater than that predicted from gravitational settling alone. This effect is enhanced for the effective impact velocity $w_{i,\mathrm{eff}}$ due to the cube of the velocity fluctuations (Figure 2a). Both w_i and w_s are smaller than w_{st} for the gravel because the fall distance is not sufficient for particles to reach terminal settling velocity.

[39] Turbulence has a much stronger effect on the predicted impact velocities for the sand owing to the large transport stage (Figure 2b). A substantial portion of the distribution of turbulent fluctuations is within the regime $w' + w_s < 0$. Because impact velocities must be positive, the distribution is truncated at $w' + w_s = 0$ before integrating. This results in an asymmetric distribution, and an average impact velocity and effective impact velocity that are much greater than the gravitational settling velocity (i.e., $w_{i,\mathrm{eff}} > w_i > w_s$) (Figure 2b). The fall distance is sufficient for the sand that the gravitational fall velocity is equal to the terminal settling velocity (i.e., $w_s = w_{st}$).

[40] The velocities calculated above are a function of transport stage for the case of particles falling from the top of the bed load layer (i.e., $H_f = H_b$) (Figure 3). For gravitational settling (w_s), the velocity increases as the bed load layer height increases (equation (25)) until a transport stage of about 10, beyond which particles are calculated to fall at the terminal velocity. The average impact velocity w_i and the effective impact velocity $w_{i,\mathrm{eff}}$ are nearly equal to the gravitational settling velocity for low transport stages ($\tau_*/\tau_{*c} < 10$) because u_* is small. However, these velocities deviate significantly from the gravitational settling velocity where $w_s - u_* < 0$ because the distribution in particle velocities becomes increasingly asymmetric. The result is that w_i and $w_{i,\mathrm{eff}}$ are significantly greater than the terminal settling velocity for large transport stages. Note that all velocity measures calculated herein (i.e., w_s, w_i, and $w_{i,\mathrm{eff}}$) converge with the predictions of the empirical equation (29) at low transport stages, which is expected since this is the regime in which it was calibrated. Equation (29) predicts an impact velocity of zero at large transport stages (i.e., $u_* > w_{st}$), which contrasts with the velocity model proposed herein.

4.5. Bedrock Erosion by Total Load

[41] Finally, to calculate the erosion rate, $w_{i,\mathrm{eff}}$ replaces w_i in equation (19) resulting in

$$E = \frac{A_1 \rho_s Y}{k_v \sigma_T^2} \frac{q w_{i,\mathrm{eff}}^3}{(UH\chi + U_b H_b)} \left(1 - \frac{q_b}{q_{bc}}\right). \quad (36)$$
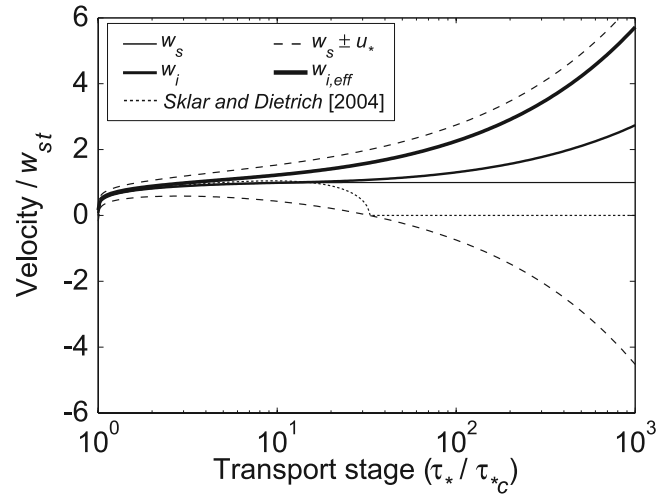
Figure 3. Calculated particle velocities relative to the terminal settling velocity (w_{st}) as a function of transport stage for 60-mm particles falling from the top of the bed load layer. Also shown by dashed lines is the settling velocity plus and minus one standard deviation due to turbulent fluctuations, where $\sigma_w = u_*$. The gravitational settling velocity (w_s) was calculated from equation (30) and approaches the terminal settling velocity at large transport stages. The calculated impact velocity (w_i) and effective impact velocity ($w_{i,\mathrm{eff}}$) deviate from w_s at large transport stages where turbulence becomes significant. The impact velocity according to *Sklar and Dietrich* [2004] goes to zero at a transport stage of about 30. The plot would be slightly different, but qualitatively similar, for different particle sizes due to changes in the drag coefficient.

Equation (36) can by nondimensionalized as

$$E^* = \frac{E\sigma_T^2}{\rho_s Y(gD)^{3/2}} = \frac{A_1}{k_v}\left[\frac{q}{(UH\chi + U_b H_b)}\right]\left[\frac{w_{i,\mathrm{eff}}}{(gD)^{1/2}}\right]^3\left[1 - \frac{q_b}{q_{bc}}\right]. \quad (37)$$

This reveals that E^* is a function of the three dimensionless quantities shown in brackets: (1) the normalized sediment supply or equivalently the near-bed sediment concentration (see equation (18)), (2) the normalized effective impact velocity cubed, and (3) the relative supply of bed load. By introducing the empirical expressions proposed in section 4, E^* also can be shown to be a function of particle size, transport stage, relative sediment supply (q/q_{bc}), and channel-bed slope (or equivalently flow depth for a given transport stage). The dependency on flow depth and channel slope was not revealed in the saltation-abrasion model (equation (6)). In the total load model, it arises because both the near-bed sediment concentration and the gravitational fall velocity are sensitive to the vertical distribution of sediment in the water column, which in turn is a function of flow depth.

5. Model Results

[42] Model results are shown for the two cases, where the total load is composed of either 60-mm gravel or 1-mm
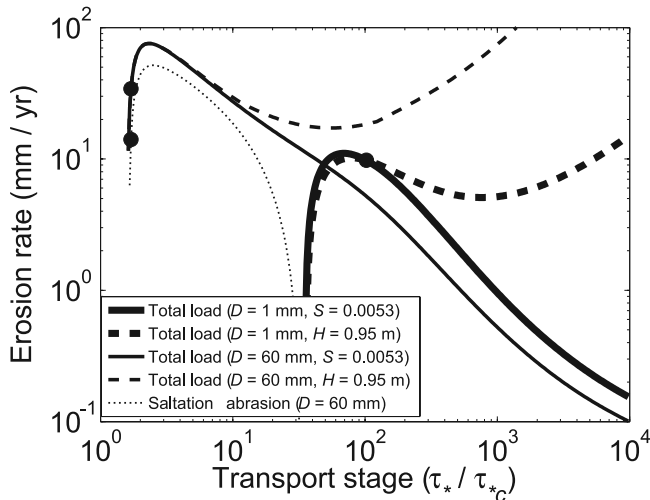
Figure 4. Log-log plot of erosion rate as a function of transport stage for 60-mm gravel and 1-mm sand. Two cases are shown for each particle size. For the first, shown by solid lines, the channel slope is $S = 0.0053$ and the flow depth varies with transport stage. For the second case, shown by dashed lines, the flow depth is $H = 0.95$ m and the channel slope varies with transport stage. For all cases, the sediment supply is 8.9×10^{-4} m^2/s. The saltation-abrasion model is shown only for 60-mm gravel because it predicts near zero erosion for the 1-mm sand at all transport stages. The black circles are the conditions for the representative field case of the Eel River (Table 1).

[45] For 60-mm gravel, the total load model predicts zero erosion at transport stages $\tau_*/\tau_{*c} \leq 1.5$ (Figure 4) because the transport capacity is less than the supply of sediment (Table 1), and the bed is therefore predicted to be covered with sediment. As transport stage increases, the rate of erosion increases as the bedrock becomes rapidly exposed. The rate of erosion initially peaks at $\tau_*/\tau_{*c} \approx 2.5$ with an erosion rate of ~70 mm/a. For larger transport stages (but smaller than $\tau_*/\tau_{*c} \approx 50$) the models predict a decreasing erosion rate with transport stage (Figure 4). This is because, for a constant sediment load, more sediment is held in the upper water column (i.e., χ and H_b increase in equation (18)), sediment is advected over the bed at a faster rate (i.e., U and U_b increase in equation (18)), and therefore the near-bed sediment concentration and the impact rate per unit bed area decrease with increasing transport stage.

[46] The decrease in sediment concentration with increasing transport stage is more significant for the constant slope case as compared to the constant depth case (Figure 5). An increased flow depth, in addition to transport stage, results in a reduction in near-bed sediment because a greater suspended load can be transported (i.e., H increases equation 18). In calculating the erosion rate, however, the reduction in c_b is offset by the increasing impact velocity with transport stage (Figure 3). For the constant depth case, the increased impact velocity more than compensates for the decrease in c_b at large transport stages ($\tau_*/\tau_{*c} > ~50$), resulting in an ever increasing erosion rate with transport stage for steep slopes ($S > ~0.15$) (Figure 4). Where slope is held constant, the erosion rate decreases (but remains nonzero) with increasing transport stage.

sand. The predicted erosion rates are given in millimeters per year; however, these rates are instantaneous and have not been multiplied by an appropriate intermittency factor for events that cause erosion. For the representative event of the South Fork Eel River, the instantaneous erosion rates for the gravel and sand are predicted to be 31 and 10 mm/a (Table 1), respectively. This yields an annual average erosion rate of 1.9 and 0.6 mm/a using an appropriate intermittency factor for the Eel River of 0.06 (see *Sklar* [2003] and *Sklar and Dietrich* [2004] for details). These predicted erosion rates seem reasonable given the average landscape lowering rate of 0.9 mm/a [*Merritts and Bull*, 1989].
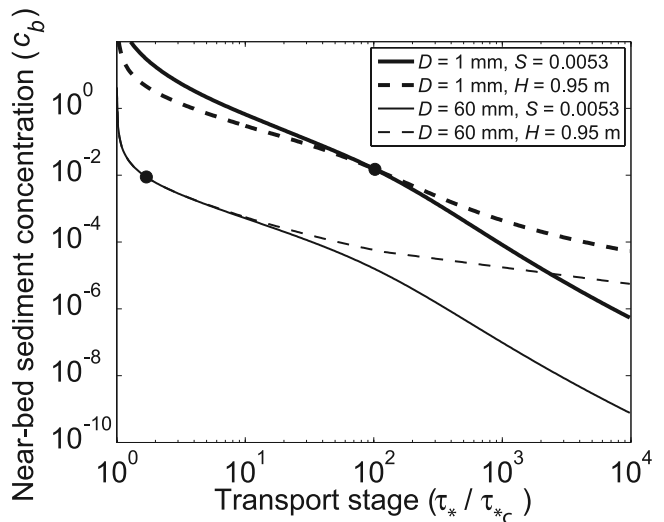
[43] To explore model predictions over a wide range of parameter space, we vary sediment supply, flow depth, or channel slope for a given grain size and hold the other variables to constant values specified for the Eel River (Table 1). In addition to our total load erosion model, the predictions of the saltation-abrasion model are shown for comparison, and we set $A_1 = A_2 = 0.36$. The integrals in equations (22), (28), (32), (34), and (35) are solved numerically.

5.1. Effect of Transport Stage

[44] For a given grain size and absolute sediment supply (Table 1), the erosion rate is a function of transport stage, which in turn is a function of channel slope and flow depth. The dependence of erosion rate on transport stage is explored here for a constant slope example (solid lines in Figure 4; $S \equiv \tan \theta = 0.0053$) and a constant flow depth example (dashed lines in Figure 4; $H = 0.95$ m).

Figure 5. Log-log plot of near-bed sediment concentration as a function of transport stage for 60-mm gravel and the 1-mm sand. Two cases are shown for each particle size. For the first, shown by solid lines, the channel slope is $S = 0.0053$ and the flow depth varies with transport stage. For the second case, shown by dashed lines, the flow depth is $H = 0.95$ m and the channel slope varies with transport stage. For all cases, the sediment supply is 8.9×10^{-4} m^2/s. The black circles are the conditions for the representative field case of the Eel River (Table 1).
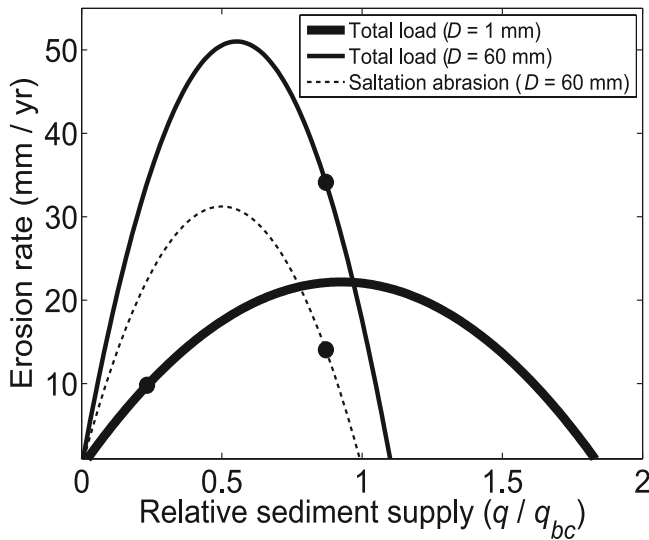
Figure 6. Erosion rate as a function of relative sediment supply for 60-mm gravel and 1-mm sand for the same hydraulic conditions (i.e., bed shear stress, flow depth, channel slope, and flow velocity (Table 1)). This corresponds to a transport stage of 1.7 and 102 for the gravel and sand, respectively. The saltation-abrasion model is shown only for 60-mm gravel because it predicts near zero erosion for the 1-mm sand at all transport stages. The black circles are the conditions for the representative field case of the Eel River (Table 1).

[47] Predictions for the 1-mm sand are qualitatively similar to the gravel (Figure 4). The bed is predicted to be covered for $\tau_*/\tau_{*c} < \sim 25$ and the initial peak in erosion rate (~ 10 mm/a) occurs at $\tau_*/\tau_{*c} \approx 100$. The magnitude of erosion is smaller for the sand as compared to the gravel because of its lower gravitational settling velocity. For the constant depth case, the erosion rate again increases with transport stage for large transport stages ($\tau_*/\tau_{*c} > \sim 10^3$) equivalent to $S > \sim 0.05$.

[48] The saltation-abrasion model for the 60-mm gravel is qualitatively similar to the total load model for small transport stages (Figure 4). The total load model peaks at a slightly higher erosion rate because of the different formulation of the impact velocity (i.e., equation (35) versus equation (29)). At large transport stages the saltation-abrasion model differs from the total load model because it forces the erosion rate to zero at $u_*/w_{st} = 1$, which corresponds to $\tau_*/\tau_{*c} \approx 35$. For 1-mm sand, the saltation-abrasion model predicts zero erosion for almost all transport stages because there is only a narrow range in which the bed is exposed and $u_*/w_{st} < 1$.

5.2. Effect of Sediment Supply

[49] With constant values of transport stage, flow depth, and channel slope (Table 1), the saltation-abrasion model predicts a peak in erosion rate where the supply of sediment is one half the bed load transport capacity (i.e., $q/q_{bc} = 0.5$) (Figure 6). The erosion rate goes to zero where the sediment supply is zero because there are no particle impacts. At high relative supply, the erosion rate also goes to zero because of bed coverage. This upper limit is $q/q_{bc} = 1$ for the saltation-abrasion model because all of the supplied sediment is

assumed to travel as bed load (i.e., $q = q_b$). The total load model, however, indicates that erosion is possible where the supply exceeds the bed load capacity because some of the load is transported in suspension (Figure 6). Thus, the bed load flux q_b can be less than the bed load capacity, even though the total load q is not. This effect is more pronounced for the sand than for the gravel because a greater proportion of the sediment load is traveling in suspension (because of the higher transport stage). Erosion persists for the sand until the supply is nearly double the bed load transport capacity (Figure 6).

5.3. Effect of Grain Size

[50] Where sediment supply, flow depth and channel slope are set to constant values for the reference field site (Table 1), the models predict a peak in erosion rate for particle sizes of about $D = 45$ mm (Figure 7). The erosion rate goes to zero for larger grain sizes because the flow is not competent to transport these sizes, such that the bed is predicted to be covered with alluvium. Because of the dependence of erosion rate on gravitational settling velocity, the erosion rate also decreases for finer grain sizes. The saltation-abrasion model predicts zero erosion for sizes smaller than about 2 mm because $u_*/w_{st} > 1$. In contrast, the total load model predicts a finite erosion rate for all particle sizes.

5.4. Effect of Flow Depth and Channel Slope

[51] In contrast to the saltation-abrasion model, the total load model is a function of flow depth, or channel slope for a given transport stage (Figure 8). Flow depth affects the erosion rate in two competing ways. On one hand, the impact rate depends on the near-bed sediment concentration, which, among other things, is a function of flow depth. For the same bed shear stress, particle size and sediment supply, a deeper flow on a smaller slope will have less sediment near the bed and a lower impact rate than a shallower flow on a steeper slope. On the other hand, for particles that do not attain
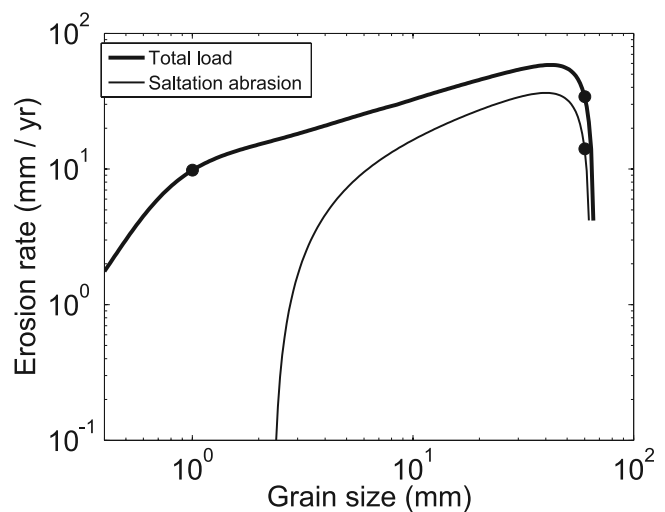
Figure 7. Log-log plot of erosion rate versus grain size for a constant flow depth ($H = 0.95$ m), channel slope ($S = 0.0053$), and sediment supply (8.9×10^{-4} m^2/s). The black circles are the conditions for the representative field case of the Eel River (Table 1).
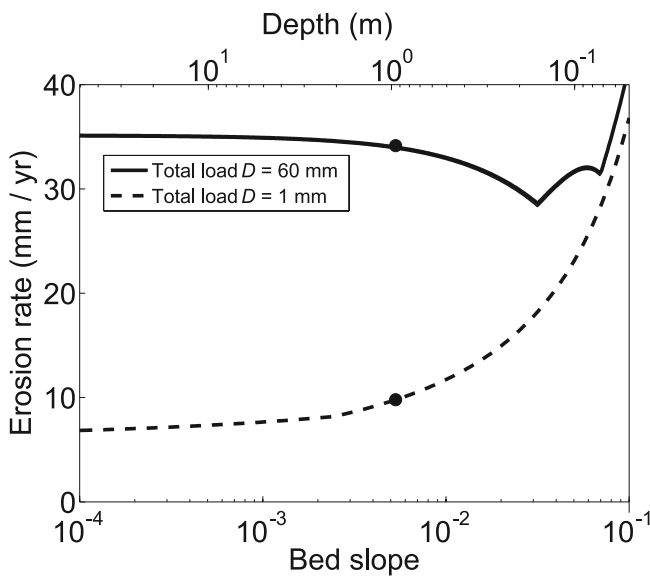
Figure 8. Erosion rate as a function of channel slope and flow depth for the 60-mm gravel (with a constant transport stage of 1.7) and the 1-mm sand (with a constant transport stage of 102) using a constant sediment supply (8.9×10^{-4} m^2/s). The saltation-abrasion model would plot as a horizontal line because it is not sensitive to the relative contributions of slope and flow depth in setting the transport stage. The black circles are the conditions for the representative field case of the Eel River (Table 1).

terminal velocity, the particle impact velocity is larger in deeper flows because of the greater fall distance.

[52] For 60-mm gravel with a constant transport stage and sediment supply, the erosion rate is nearly constant at low channel slopes, but decreases as slope increases (Figure 8). For this sediment size, the increased impact rate in shallower and steeper flows is more than compensated for by the drop in impact velocity (because of the reduced fall distance), resulting in a decrease in erosion rate with increasing slope. In contrast, finer sediment rapidly reaches terminal velocity so that changes in flow depth have little effect on impact velocity. Thus, the erosion rate for 1-mm sand is predicted to increase with increasing slope because of the greater impact rate that results from the increased near-bed sediment concentration in steeper flows with smaller flow depths (Figure 8).

[53] The abrupt increase in erosion rate for the gravel at $S \approx 0.04$ and $H \approx 0.2$ m (Figure 8) occurs where the bed load velocity given by equation (24) is predicted to be larger than the fluid velocity (equation (22)), and therefore we set $U_b = U$ (see section 4.2). The jump in erosion rate is because the bed load velocity is predicted to increase with transport stage (regardless of flow depth), whereas U systematically decreases with increasing slope (and decreasing flow depth). This results in a heightened near-bed sediment concentration and erosion rate. The second jump in erosion rate at $S \approx 0.07$ and $H \approx 0.07$ m (Figure 8) is where $H_b = H$, which again results in a heightened near-bed sediment concentration with increasing slope (and decreasing flow depth).
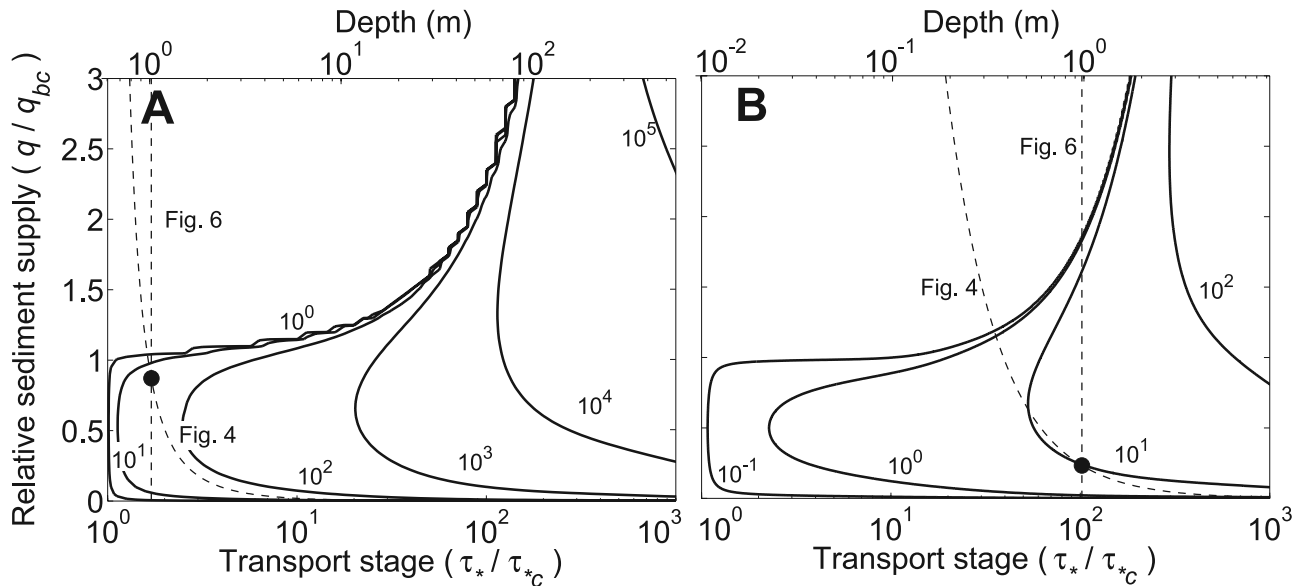
5.5. Contour Plots of Erosion Rate

[54] To evaluate the total load model over a wide range of parameter space, Figures 9–11 show contours of erosion rate versus transport stage and relative sediment supply. The saltation-abrasion model shows a peak erosion rate at a relative sediment supply of 0.5 and a transport stage of $\tau_*/\tau_{*c} \approx 15$ for both the 1-mm sand and the 60-mm gravel (Figure 9). The peak erosion rate occurs at a slightly different transport stage for the two different sediment sizes because the relationship between transport stage and the onset of suspension is a function of the drag coefficient, which is grain-size dependent [*Dietrich*, 1982]. The erosion rate goes to zero at high and low transport stages because of the onset of suspension and the threshold of motion, respectively. The erosion rate goes to zero at high and low relative sediment supply because of the effects of bedrock coverage and particle impact rate, respectively (see *Sklar and Dietrich* [2004] for a detailed discussion).

[55] The contour plots of the total load erosion model are strikingly different than the model that considers only bed load (Figures 10 and 11). Like the bed load model, the
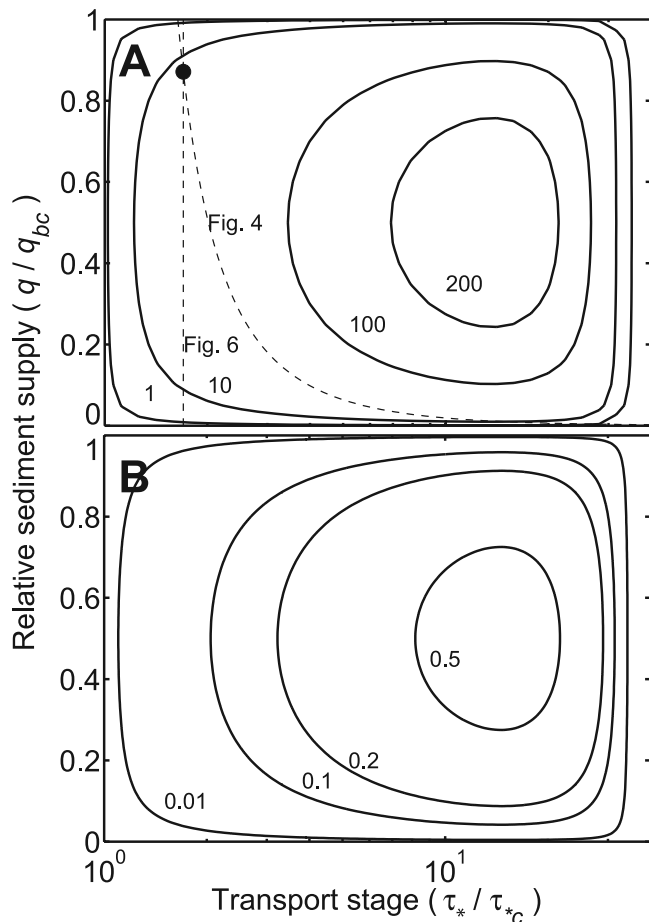
Figure 9. Contour plots of erosion rate in millimeters per year for the saltation-abrasion model versus transport stage and relative sediment supply for (a) 60-mm gravel and (b) 1-mm sand. The dashed lines are slices through parameter space that are shown on Figures 4 and 6. The black circles are the conditions for the representative field case of the Eel River (Table 1).

Figure 10. Contour plots of erosion rate in millimeters per year predicted by the total load erosion model for (a) 60-mm gravel and (b) 1-mm sand. The dashed lines are slices through parameter space that are shown on Figures 4 and 6. The black circles are conditions for the field case of the Eel River (Table 1). The channel slope is held constant at $S = 0.0053$, so that transport stage is a function of flow depth. Note that 3 orders of magnitude in transport stage are explored here, versus only $\sim$1 order of magnitude in Figure 9. For the 60-mm gravel, the large transport stages shown correspond to unrealistic flow depths for the Eel River (see discussion in section 6.3) but are shown for sake of comparison with the 1-mm sand.

erosion rate increases with increasing transport stage (with a constant channel slope) because the impact velocity increases with increasing flow depth (Figure 10). The erosion rate, however, does not decline at large transport stages for a given relative sediment supply. Instead, it increases because of the heightened impact velocity due to turbulence. The dashed lines on Figure 10 show the 2-D parameter space represented in Figures 4 and 6. These illustrate that an increase in transport stage results in a decrease in relative supply (q/q_{bc}), if the absolute sediment supply (q) is constant. This is the reason for the decrease in erosion rate at high transport stages in Figure 4. The contour plots, however, reveal that erosion rate can increase indefinitely with increasing transport stage, as long as the absolute sediment supply also increases with transport stage. In such a case, the erosion rate does not have a maximum value (Figure 10). Furthermore, at large transport stages ($\tau_*/\tau_{*c} > 100$), the erosion rate can be nonzero for sediment loads that are much larger than the bed load transport capacity.

[56] The dependencies of erosion rate on transport stage differ where flow depth is held constant rather than channel slope (Figure 11). The predictions for the sand (Figure 11b) are qualitatively similar to the cases with constant channel slope (Figure 10). However, as discussed in section 5.1, the erosion rate is generally greater if depth is held constant, rather than slope, because the near-bed sediment concentration (and therefore impact rate) is a function of flow depth. This allows, for example, an ever increasing erosion rate with transport stage for large transport stages ($\tau_*/\tau_{*c} > \sim$50), even if the absolute sediment supply is constant (Figures 5 and 11b). For the 60-mm gravel, the erosion rate is predicted

to be zero for values of the relative sediment supply greater than about unity (Figure 11a). This is because, for the large slopes considered here, the bed load layer height predicted by equation (25) exceeds the flow depth, which results in zero flux of suspended sediment since the bed load layer occupies the entire water column.

6. Discussion

6.1. Entrainment Capacity for Total Load

[57] Equation (36) contains a transport capacity for bed load q_{bc}, in which erosion is zero if $q_b > q_{bc}$ because of depositional cover. For flows with significant suspended sediment, the transport capacity of the total load is typically formulated in terms of a maximum near-bed sediment concentration instead of a maximum bed load flux [*Smith and McLean*, 1977; *Parker*, 1978; *García and Parker*, 1991]. This maximum sediment concentration can be found by equating equations (11) and (16), i.e., $c_b = \alpha$, as discussed in section 3.3. For most of the model results shown, the near-bed sediment concentration does not exceed α, where α is calculated using the empirical model of *García and Parker* [1991]. This, however, is not true for the 1-mm sand at small transport stages. For $\tau_*/\tau_{*c} < \sim$10, the bed is predicted to be covered with sediment (i.e., $c_b > \alpha$) and thus the erosion rate is zero (Figure 12). This indicates a need for an accurate model of the maximum near-bed sediment concentration for both bed load and suspension conditions, and particularly the transition in between.

6.2. Viscous Damping of Impacts

[58] *Sklar and Dietrich* [2004] assumed that there was not a threshold kinetic energy required to cause erosion in their
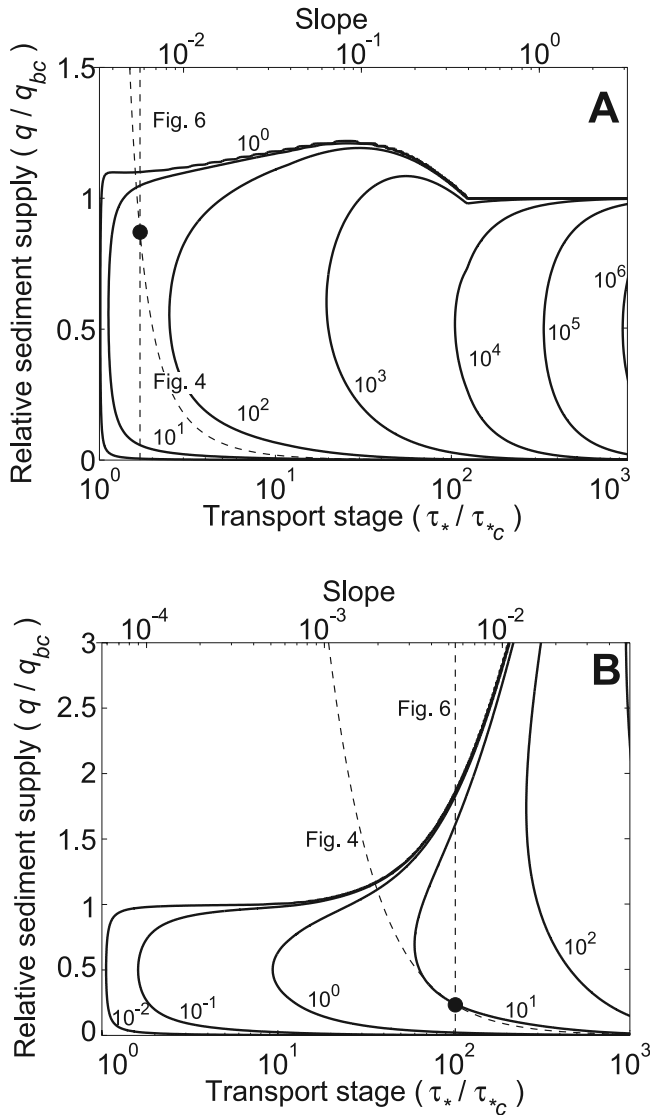
Figure 11. Contour plots of erosion rate in millimeters per year for the total load erosion model for (a) 60-mm gravel and (b) 1-mm sand. The dashed lines are slices through parameter space that are shown on Figures 4 and 6. The black circles are conditions for the field case of the Eel River (Table 1). The flow depth is held constant at $H = 0.95$ m, so that the transport stage is a function of channel slope. The vertical axes differ for the 60-mm gravel and the 1-mm sand.

model on the basis of abrasion mill experiments [*Sklar and Dietrich*, 2001], an assumption that we adopted in the total load erosion model. Nonetheless, considering the fine particles addressed here, it is possible that some impacts might be viscously damped. Theoretical and experimental results suggest that particle-wall impacts can be viscously damped, and the degree to which is a function of the particle Stokes number [*Davis et al.*, 1986; *Lian et al.*, 1996; *Schmeeckle et al.*, 2001; *Joseph and Hunt*, 2004]. For spheres impacting a wall, the Stokes number can be written as

$$St = \frac{\rho_s w_p D}{9 \rho_f \nu} \qquad (38)$$

and is a measure of the particle inertia relative to the viscous force exerted on the particle from the fluid, where ν is the kinematic viscosity of the fluid (10^{-6} m^2/s) and w_p is the particle velocity. Both *Schmeeckle et al.* [2001] and *Joseph and Hunt* [2004] found that impacts from glass spheres were partially damped for $St < {\sim}100$, and completely damped for $St < {\sim}30$. *Schmeeckle et al.* [2001] also show that data are more scattered for natural sediment because of their nonspherical nature.

[59] If the erosion rate is set to zero for particle impacts with $St < 30$ (where $w_p = w' + w_s$ in equation (25)), the 1-mm sand is predicted to cause no erosion for transport stages less than about 3 (Figure 13a). For larger transport stages the sand does erode the bed because the enhanced impact velocity due to turbulence increases the Stokes number to $St > 30$. Viscous damping apparently has no effect on the 60-mm gravel because the gravitational settling velocity is great enough that $St > 30$ for all transport stages.

[60] To assess a potential threshold energy needed to cause erosion, it is useful to compare the model predictions to the abrasion mill experiments of *Sklar and Dietrich* [2001] (Figure 13b). The experiments were performed by mechanically stirring sediment and water in a cylindrical basin with a bedrock floor. Particle size was varied whereas the total volume of sediment, which is equivalent to q in a closed system, was held constant. The saltation-abrasion model matches the data well for large particle sizes, but predicts zero erosion for the medium sand ($D = 0.4$ mm) because it was in suspension. The total load erosion model, on the other hand, captures the measured finite erosion for the medium sand (Figure 13b), but over predicts the erosion rate. Although the fit seems better by including a Stokes number cutoff (Figure 13b), it is nonetheless difficult to evaluate whether the data support this threshold. For example, *Sklar and Dietrich* [2004] reported that fine sand ($D = 0.2$ mm) did not produce wear above their detection limit (${\sim}10^{-3}$ g/h),
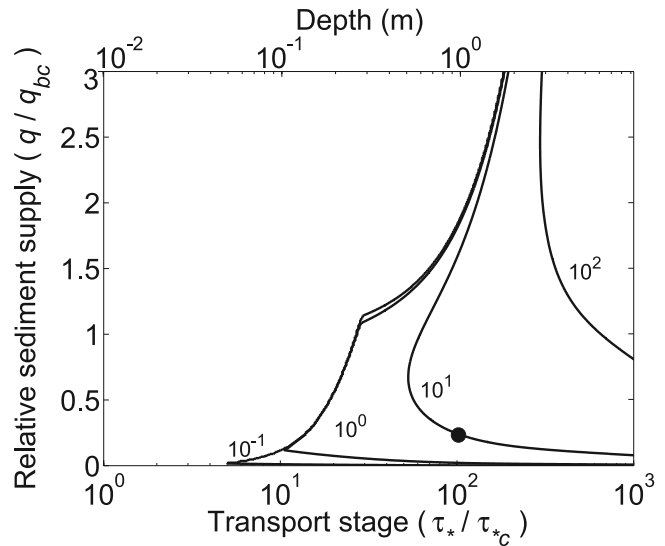
Figure 12. Contour plot of erosion rate in millimeters per year for the same model parameters as Figure 10b, except that erosion rate is set to zero where the near-bed sediment concentration exceeds the entrainment capacity of the flow (i.e., $c_b > \alpha$). The black circle represents the conditions for the field case of the Eel River (Table 1).
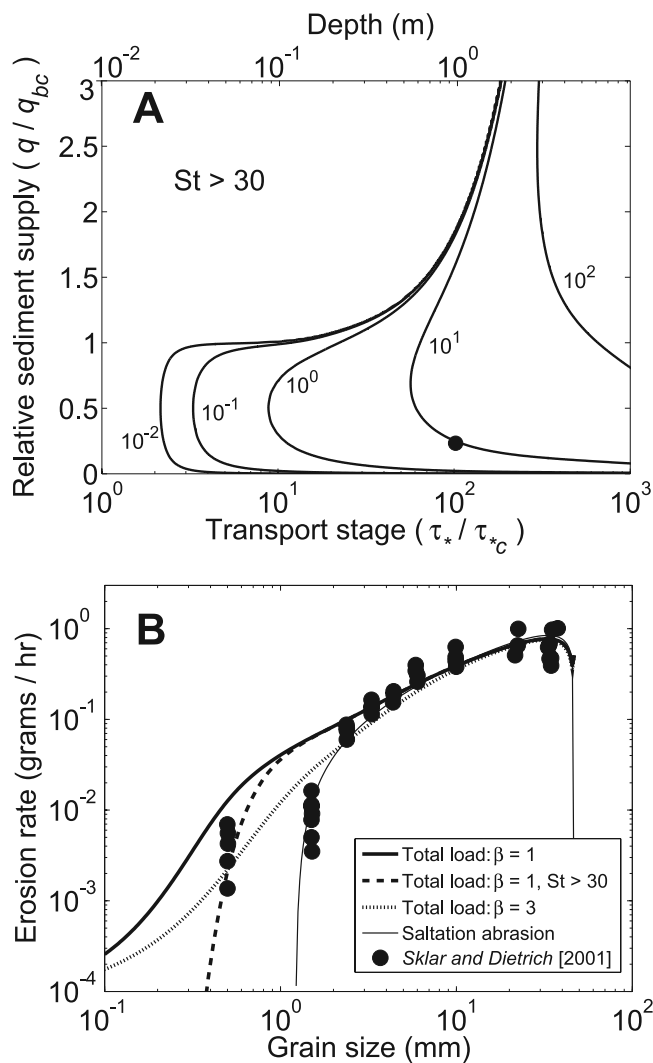
Figure 13. (a) Contour plot of erosion rate in millimeters per year for the same model parameters as Figure 10b, except that the erosion rate is set to zero if particle impacts have a particle Stokes number less than 30. The black circle represents the conditions for the field case of the Eel River (Table 1). (b) Comparison of the total load erosion model and the saltation-abrasion model with the experimental abrasion mill data of *Sklar and Dietrich* [2001]. To make these calculations $A_1 = 0.2$, $H = 0.5$ m, $k_v = 3 \times 10^{-5}$, $\sigma_T = 9$ MPa, $u_* = 0.15$ m/s, $q = 4.2 \times 10^{-4}$ m^2/s, and the cover term was neglected (see *Sklar and Dietrich* [2004] for more details).

but this is also consistent with the predictions of the total load erosion model both with or without the Stokes number cutoff. Furthermore, it is not obvious that the formulations used herein (i.e., the parabolic eddy viscosity: equation (27)) should hold for the abrasion mill where flow was driven by a propeller and strong secondary currents developed. The model fit, for example, is improved by setting $\beta = 3$ in equation (27) (Figure 13b).

6.3. Implications for Natural Streams

[61] The total load erosion model differs significantly from the saltation-abrasion model for high transport stages and high relative sediment supply rates. The large transport stages explored for the 60-mm gravel (e.g., $\tau_*/\tau_{*c} \gg 1$) most likely occur during relatively large floods or in steep mountain terrain. For example, the bed shear stress for the Bonneville flood of the western United States has been estimated to be 2500 Pa [*O'Connor*, 1993]. We calculate that this flood was competent to suspend 150-mm cobbles (i.e., $u_*/w_{st} = 1$, using the w_{st} relation of *Dietrich* [1982] for natural sediment), which is consistent with Bonneville flood deposits [*O'Connor*, 1993]. During this event, 60-mm gravel was at a transport stage of $\tau_*/\tau_{*c} = 85$, and 1-mm sand was at $\tau_*/\tau_{*c} = 5.2 \times 10^3$. In mountain terrains, such large bed stresses can be achieved more readily. For example, during Typhoon Bilis in 2000, which has a recurrence interval of about 20 years, the reach averaged bed stress of the LiWu River in Taiwan was about 2300 Pa [*Hartshorn et al.*, 2002], making this more frequent event nearly as competent as the Bonneville flood in suspending gravel. In fact, the maximum across channel erosion rates during Typhoon Bilis occurred several meters above the channel thalweg, suggesting that erosion by suspended particles outpaced bed load [*Hartshorn et al.*, 2002].

[62] The total load erosion model is also important to consider for fine sediment, which can be at large transport stages during more regular flow events. For the characteristic event on the Eel River, the 1-mm sand is calculated to have a transport stage of $\tau_*/\tau_{*c} = 102$. For these conditions the saltation-abrasion model predicts no erosion, whereas the total load model predicts an instantaneous erosion rate of approximately 10 mm/a. The erosion rate due to sand is smaller than that predicted for gravel (for the same sediment supply), but it is nonetheless significant (Table 1). The total load model might be particularly important for rivers where the load is dominated by sand, for example, because of granite or sandstone lithologies.

[63] Deciphering between the relative roles of sand and gravel in fluvial erosion is beyond the scope of this paper. A significant limitation of the model is that it only considers sediment of a single size. It is clear from evaluation of the contour plots (Figures 10 and 11), that there are regimes in parameter space where erosion from sand can be greater than that from gravel, but this depends on the relative supply of each. Since finer particles often dominate the load of a river, it seems possible that erosion from sand might be as or more important than erosion from gravel. Incorporating multiple particle sizes and particularly bimodal distributions of sediment into the model, however, is not trivial. For example, it has been shown that the addition of sand into a gravel bed can lead to nonlinear increases in the transport capacity of both sizes [*Wilcock et al.*, 2001; *Wilcock and Crowe*, 2003]. Extending the erosion model to multiple particle sizes would require reassessment of several formulas used herein to account for mixture and bimodal effects (over a bedrock bed) including the bed load transport capacity, the hydraulic roughness of the bed, the bed load velocity and the bed load layer height. Experimental and field measurements are needed to guide future theoretical work.

[64] The total load erosion model is most sensitive to the prediction of impact velocity, and this is also a topic that deserves future study. For example, our characterization of particle fluctuations as a Gaussian distribution is undoubtedly oversimplified. The degree to which particles detach

from the fluid near the boundary likely depends on the relative particle response time compared to the fluid turbulence timescale (i.e., a particle Stokes number) [e.g., *Crowe et al.*, 1996]. In addition, local turbulent fluctuations can be intense, especially above a nonuniform bed. The model does not incorporate changes in hydraulic roughness or turbulence due to sediment cover or bed forms. Erosion of protruding pieces of bedrock is likely to be much more efficient than erosion into a flat bed (as assumed herein), because the impact velocity should scale with the mean flow rather than turbulence intensity or the settling velocity [e.g., *Anderson*, 1986]. Furthermore, erosion by suspended sediment could be substantial over bed forms such as flutes or potholes, where there is a significant advective component of the impact velocity by the mean flow or vortices [*Alexander*, 1932; *Tinkler*, 1997; *Whipple et al.*, 2000; *Johnson and Whipple*, 2007].

[65] Where it differs from the saltation-abrasion model, the total load erosion model should have significant implications for predicting river channel morphology. For example, variations of the saltation-abrasion model have been used to model knickpoint migration in bedrock rivers [e.g., *Chatanantavet and Parker*, 2005; *Gasparini et al.*, 2007; *Crosby et al.*, 2007], and the total load model is likely to make different predictions owing to the large transport stages that typify these steepened reaches. It has been suggested, for example, that hanging valleys might form because, on the basis of the saltation-abrasion model, steepened reaches have lower erosion rates because of increased particle hop lengths and decreased impact rates [*Wobus et al.*, 2006; *Crosby et al.*, 2007]. The total load erosion model, however, suggests the opposite: erosion rates increase with increasing channel slope and transport stage (at least for large transport stages, e.g., Figure 4) because of the advection of suspended particles toward the bed by turbulent eddies. Some support for this finding comes from the experiments of *Chatanantavet and Parker* [2006], where the erosion rate was found to increase with increasing slope, even for the case of a constant transport stage.

[66] Although the total load erosion model offers insight into channel dynamics, we caution against using it (or other fluvial abrasion models) for quantitative estimates in steep reaches with large roughness to depth ratios (i.e., k_s/H). In these cases, descriptions of flow resistance [e.g., *Bathurst*, 1985], sediment transport capacity [*Yager et al.*, 2007], and incipient sediment motion [*Lamb et al.*, 2008] are likely to be different that the formulas used herein. Moreover, at near vertical slopes, other processes such as plunge pool erosion [e.g., *Lamb et al.*, 2007] are probably more important than fluvial abrasion.

7. Conclusions

[67] We have developed a mechanistic model for fluvial bedrock incision by suspended and bed load sediment. Particles are considered to impact the bed because of gravitational settling and advection by turbulent eddies, the latter of which dominates at high transport stages. The model predicts that the erosion rate is a function of three dimensionless quantities for a given grain size: transport stage (τ_*/τ_{*c}), relative sediment supply (q/q_{bc}), and channel slope. Inclusion of suspension is important for high trans-

port stages (i.e., large floods, steep slopes, or small particle sizes) and high relative sediment supply rates. For a given ratio of sediment supply to transport capacity, the erosion rate is predicted to increase with transport stage because of the heightened impact velocity due to turbulent fluctuations and does not taper to zero as predicted in the saltation-abrasion model. For most cases, erosion rates increase more rapidly with transport stage by increasing slope and fixing depth, rather than the opposite. This depth (or slope) dependency on erosion rate arises because both the near-bed sediment concentration and the particle fall velocity are sensitive to the vertical distribution of sediment in the water column. The total load erosion model predicts that erosion can be substantial where the sediment supply exceeds the bed load transport capacity because a portion of the load is carried in suspension.

Appendix A: Fall Velocity

[68] The acceleration of a falling particle can be calculated from the difference between the gravitational acceleration of the particle and deceleration due to drag

$$\frac{dw}{dt} = C_1 - C_2 w^2, \tag{A1}$$

where w is velocity in the vertical dimension, g is the acceleration due to gravity and C_1 and C_2 are given by

$$C_1 = \frac{(\rho_s - \rho_f)}{\rho_s} g \tag{A2}$$

$$C_2 = \frac{1}{2} C_d \frac{\rho_f}{\rho_s} \frac{A_x}{V_p}, \tag{A3}$$

where C_d is a drag coefficient, ρ_f is the density of the fluid that the particle is falling through, ρ_s is the particle density, A_x is the cross sectional area of the particle perpendicular to fall velocity, and V_p is the volume of the particle. We are interested in the acceleration over a certain fall distance rather than over a certain fall time. Equation (A1) can be written in terms of vertical distance z (positive downward) by substituting $dt = dz/w$, which yields

$$w\frac{dw}{dz} + C_2 w^2 = C_1. \tag{A4}$$

To solve equation (A4) analytically, we assume that C_2, and therefore C_d, is not a function of z. In reality C_d should vary as particles accelerate and the particle Reynolds number increases. Using a simple numerical integration, we found that accounting for a variable drag coefficient typically has less than a 10% effect on settling velocity. We therefore assume that C_d is a constant for a given particle size and solve the nonlinear ordinary differential equation as

$$w = \sqrt{\frac{C_1}{C_2}(1 - \exp(-2C_2 z))}, \tag{A5}$$

where the boundary condition $w(z=0) = 0$ has been applied. Substituting equations (A2) and (A3) into equation (A5), assuming spherical particles (i.e., $V_p/A_x = 2D/3$), defining the

fall distance as $z = H_f/\cos\theta$, and taking the component normal to the bed results in equation (30).

Notation

A_x cross sectional area of a sediment particle (L^2);
c volumetric sediment concentration (dimensionless);
c_b near-bed volumetric sediment concentration (dimensionless);
C_d drag coefficient (dimensionless);
D sediment diameter (L)
E rate of vertical erosion (LT^{-1})
I_r impact rate per unit bed area ($L^{-2}T^{-1}$)
F_e fraction of exposed bedrock (dimensionless);
g acceleration due to gravity (LT^{-2})
H depth of flow (L)
H_b thickness of the bed load layer (L)
H_f particle fall distance (L)
L_b particle saltation hop length (L)
n roughness coefficient (dimensionless);
P rouse parameter (dimensionless);
q volumetric sediment supply per unit channel width (L^2T^{-1})
q_b volumetric bed load flux per unit channel width (L^2T^{-1})
q_{bc} volumetric bed load transport capacity per unit channel width (L^2T^{-1})
q_s volumetric suspended load flux per unit channel width (L^2T^{-1})
q_w volumetric water discharge per unit channel width (L^2T^{-1})
R submerged specific density of sediment (dimensionless);
S channel-bed slope (dimensionless);
St particle Stokes number (dimensionless);
t_i time between particle impacts (T)
u stream-wise flow velocity (LT^{-1})
U depth-averaged stream-wise flow velocity (LT^{-1})
U_b depth-averaged stream-wise bed load velocity (LT^{-1})
u_* shear velocity (LT^{-1})
V_i volume of eroded rock per impact (L^3)
V_p volume of a particle (L^3)
W channel width (L)
w vertical velocity (LT^{-1})
w_{st} terminal settling velocity of a particle (LT^{-1})
w_i impact velocity of a particle at the bedrock interface (LT^{-1})
$w_{i,\text{eff}}$ effective impact velocity (LT^{-1})
w_p particle velocity (LT^{-1})
w_s velocity of a falling particle normal to the bed (LT^{-1})
w' velocity fluctuations perpendicular to the bed (LT^{-1})
Y Young's modulus of elasticity ($ML^{-1}T^{-2}$)
z height above the bed (L)
z_0 flow roughness parameter (L)
ε_v energy to erode a unit volume of bedrock ($ML^{-1}T^{-2}$)
σ_T rock tensile strength ($ML^{-1}T^{-2}$)
σ_w standard deviation in vertical velocity fluctuations (LT^{-1})

α sediment entrainment parameter (dimensionless);
β proportionality constant relating the diffusivity of momentum and sediment (dimensionless);
k_v empirical rock erodibility coefficient (dimensionless);
κ von Karman's constant (dimensionless);
ζ_z relative height above the bed (dimensionless);
ζ_b relative height of the bed load layer (dimensionless);
ν kinematic viscosity of the fluid (L^2T^{-1})
ν_T turbulent eddy viscosity (L^2T^{-1})
ρ_s density of sediment (ML^{-3})
ρ_f density of fluid (ML^{-3})
τ_* shields stress (dimensionless);
τ_{*c} critical Shields stress for incipient sediment motion (dimensionless);
χ integral relating the flux of suspended sediment to c_b, H, and U (dimensionless).

References

Abbott, J. E., and J. R. D. Francis (1977), Saltation and suspension trajectories of solid grains in a water stream, *Philos. Trans. R. Soc. London Ser. A*, *284*(1321), 225–254, doi:10.1098/rsta.1977.0009.

Alexander, H. S. (1932), Pothole erosion, *J. Geol.*, *40*(4), 305–337.

Anderson, R. S. (1986), Erosion profiles due to particles entrained by wind: Application of an eolian sediment-transport model, *Geol. Soc. Am. Bull.*, *97*, 1270–1278, doi:10.1130/0016-7606(1986)97<1270:EPDTPE>2.0. CO;2.

Bagnold, R. A. (1966), *An Approach to the Sediment Transport Problem From General Physics*, U.S. Geol. Surv., Washington, D. C.

Bathurst, J. C. (1985), Flow resistance estimation in mountain rivers, *J. Hydraul. Eng.*, *111*(4), 625–643.

Beaumont, C., P. Fullsack, and J. Hamilton (1992), Erosional control of active compressional orogens, in *Thrust Tectonics*, edited by K. R. McClay, pp. 1–18, Chapman and Hall, New York.

Bennett, S. J., J. S. Bridge, and J. L. Best (1998), Fluid and sediment dynamics of upper stage plane beds, *J. Geophys. Res.*, *103*(C1), 1239–1274, doi:10.1029/97JC02764.

Bridge, J. S., and S. J. Bennett (1992), A model for the entrainment and transport of sediment grains of mixed sizes, shapes, and densities, *Water Resour. Res.*, *28*(2), 337–363, doi:10.1029/91WR02570.

Buffington, J. M., and D. R. Montgomery (1997), A systematic analysis of eight decades of incipient motion studies, with special reference to gravel-bedded rivers, *Water Resour. Res.*, *33*, 1993–2029.

Carter, C. L., and R. S. Anderson (2006), Fluvial erosion of physically modeled abrasion-dominated slot canyons, *Geomorphology*, *81*, 89–113, doi:10.1016/j.geomorph.2006.04.006.

Chatanantavet, P., and G. Parker (2005), Modeling the bedrock river evolution of western Kaua'i, Hawai'I, by a physically-based incision model based on abrasion, in *River, Coastal, and Estuarine Morphodynamics: RCEM 2005*, edited by G. Parker and M. Garcia, pp. 99–110, Taylor and Francis, London.

Chatanantavet, P., and G. Parker (2006), Experimental studies on the rate of incision by saltating abrasion: Verification, analysis and revision of a physically-based model, *Eos Trans. AGU*, *87*(52), Fall Meet. Suppl., Abstract H21E–1423.

Cheng, N. S., and Y. M. Chiew (1999), Analysis of initiation of sediment suspension from bed load, *J. Hydraul. Eng.*, *125*(8), 855–861, doi:10.1061/(ASCE)0733-9429(1999)125:8 (855).

Coles, D. F. (1956), The law of the wake in turbulent boundary layer, *J. Fluid Mech.*, *1*, 191–226, doi:10.1017/S0022112056000135.

Crosby, B. T., K. X. Whipple, N. M. Gasparini, and C. W. Wobus (2007), Formation of fluvial hanging valleys: Theory and simulation, *J. Geophys. Res.*, *112*, F03S10, doi:10.1029/2006JF000566.

Crowe, C. T., T. R. Trout, and J. N. Chung (1996), Numerical models for two-phase flows, *Annu. Rev. Fluid Mech.*, *28*, 11–43, doi:10.1146/annurev.fl.28.010196.000303.

Davis, R., J. Serayssol, and E. Hinch (1986), The elastohydrodynamical collision of two spheres, *J. Fluid Mech.*, *163*, 479–497, doi:10.1017/S0022112086002392.

Dietrich, W. E. (1982), Settling velocity of natural particles, *Water Resour. Res.*, 18(6), 1615–1626, doi:10.1029/WR018i006p01615.

Dietrich, W. E., D. Bellugi, L. Sklar, J. D. Stock, A. M. Heimsath, and J. J. Roering (2003), Geomorphic transport laws for predicting landscape form and dynamics, in *Prediction in Geomorphology, Geophys. Monogr. Ser.*, vol. 135, edited by P. Wilcock and R. Iverson, pp. 1–30, AGU, Washington, D. C.

Einstein, H. A. (1968), Deposition of suspended particles in a gravel bed, *J. Hydraul. Eng.*, 94(5), 1197–1205.

Fernandez Luque, F. R., and R. van Beek (1976), Erosion and transport of bed-load sediment, *J. Hydraul. Res.*, 14, 127–144.

Finnegan, N. J., L. S. Sklar, and T. K. Fuller (2007), Interplay of sediment supply, river incision, and channel morphology revealed by the transient evolution of an experimental bedrock channel, *J. Geophys. Res.*, 112, F03S11, doi:10.1029/2006JF000569.

Foley, M. G. (1980), Bedrock incision by streams, *Geol. Soc. Am. Bull.*, 91, 2189–2213.

Francis, J. R. D. (1973), Experiments on motion of solitary grains along bed of a water-stream, *Proc. R. Soc. London Ser. A*, 332(1591), 443–471, doi:10.1098/rspa.1973.0037.

García, M. H., and G. Parker (1991), Entrainment of bed sediment into suspension, *J. Hydraul. Eng.*, 117(4), 414–435, doi:10.1061/(ASCE) 0733-9429(1991)117:4(414).

Gasparini, N. M., K. X. Whipple, and R. L. Bras (2007), Predictions of steady state and transient landscape morphology using sediment-flux-dependent river incision models, *J. Geophys. Res.*, 112, F03S09, doi:10.1029/2006JF000567.

Gelfenbaum, G., and J. D. Smith (1986), Experimental evaluation of a generalized suspended-sediment transport theory, in *Shelf Sands and Sandstones*, edited by R. J. Knight and S. R. McLean, pp. 133–144, Can. Soc. of Pet. Geol., Calgary, Alberta.

Gilbert, G. K. (1877), *Report on the Geology of the Henry Mountains*, 166 pp., U.S. Gov. Print. Off., Washington, D. C.

Graf, W. H., and M. Cellino (2002), Suspension in open channels: Experimental study, *J. Hydraul. Res.*, 40(4), 435–447.

Grass, A. J. (1970), Initial instability of fine bed sands, *J. Hydraul. Eng.*, 96, 619–632.

Hancock, G. S., R. S. Anderson, and K. X. Whipple (1998), Beyond power: Bedrock river incision process and form, in *Rivers Over Rock: Fluvial Processes in Bedrock Channels, Geophys. Monogr. Ser.*, vol. 107, edited by K. J. Tinkler and E. E. Wohl, pp. 35–60, AGU, Washington, D. C.

Hartshorn, K., N. Hovius, W. B. Dade, and R. L. Slingerland (2002), Climate-driven bedrock incision in an active mountain belt, *Science*, 297(5589), 2036–2038, doi:10.1126/science.1075078.

Howard, A. D. (1998), Long profile development of bedrock channels: Interaction of weathering, mass wasting, bed erosion, and sediment transport, in *Rivers Over Rock: Fluvial Processes in Bedrock Channels, Geophys. Monogr. Ser.*, vol. 107, edited by K. J. Tinkler and E. E. Wohl, pp. 237–260, AGU, Washington, D. C.

Howard, A. D., and G. Kerby (1983), Channel changes in badlands, *Geol. Soc. Am. Bull.*, 94(6), 739–752, doi:10.1130/0016-7606(1983)94<739: CCIB>2.0.CO;2.

Howard, A. D., W. E. Dietrich, and M. A. Seidl (1994), Modeling fluvial erosion on regional and continental scales, *J. Geophys. Res.*, 99, 13,971–13,986, doi:10.1029/94JB00744.

Hu, C. H., and Y. J. Hui (1996), Bed-load transport: Part I. Mechanical characteristics, *J. Hydraul. Eng.*, 122(5), 245–254, doi:10.1061/(ASCE) 0733-9429(1996)122:5 (245).

Jackson, R. G. (1976), Sedimentological and fluid-dynamic implications of turbulent bursting phenomenon in geophysical flows, *J. Fluid Mech.*, 77(3), 531–560, doi:10.1017/S0022112076002243.

Johnson, J. P., and K. X. Whipple (2007), Feedbacks between erosion and sediment transport in experimental bedrock channels, *Earth Surf. Processes Landforms*, 32, 1048–1062, doi:10.1002/esp.1471.

Joseph, G. G., and M. L. Hunt (2004), Oblique particle-wall collisions in a liquid, *J. Fluid Mech.*, 510, 71–93, doi:10.1017/S002211200400919X.

Kamphius, J. W. (1974), Determination of sand roughness for fixed beds, *J. Hydraul. Res.*, 12(2), 193–203.

Lamb, M. P., A. D. Howard, W. E. Dietrich, and J. T. Perron (2007), Formation of amphitheater-headed valleys by waterfall erosion after large-scale slumping on Hawaii, *Geol. Soc. Am. Bull.*, 119, 805–822, doi:10.1130/B25986.1.

Lamb, M. P., W. E. Dietrich, and J. G. Venditti (2008), Is the critical Shields number for incipient sediment motion dependent on channel-bed slope?, *J. Geophys. Res.*, 113, F02008, doi:10.1029/2007JF000831.

Lee, H. Y., and I. S. Hsu (1994), Investigation of saltating particle motions, *J. Hydraul. Eng.*, 120(7), 831–845, doi:10.1061/(ASCE)0733-9429 (1994)120:7(831).

Lian, G., M. Adams, and C. Thornton (1996), Sediment suspension with rippled bed, *J. Fluid Mech.*, 311, 141–152, doi:10.1017/ S0022112096002534.

McLean, S. R. (1992), On the calculation of suspended-load for noncohesive sediments, *J. Geophys. Res.*, 97(C4), 5759–5770, doi:10.1029/ 91JC02933.

Merritts, D., and W. B. Bull (1989), Interpreting Quaternary uplift rates at the Mendocino triple junction, northern California, from uplifted marine terraces, *Geology*, 17, 1020–1024, doi:10.1130/0091-7613(1989)017 <1020:IQURAT>2.3.CO;2.

Muste, M., K. Yu, I. Fujita, and R. Ettema (2005), Two-phase versus mixed-flow perspective on suspended sediment transport in turbulent channel flows, *Water Resour. Res.*, 41, W10402, doi:10.1029/2004WR003595.

Nelson, J. M., R. L. Shreve, D. C. McLean, and T. G. Drake (1995), Role of near-bed turbulence structure in bed load transport and bed form mechanics, *Water Resour. Res.*, 31(8), 2071–2086, doi:10.1029/ 95WR00976.

Nelson, P. A., and G. Seminara (2007), Sediment supply and the prediction of bedrock channel cross section evolution, *Eos Trans. AGU*, 88(52), Fall Meet. Suppl., Abstract H44B–04.

Nezu, I., and R. Azuma (2004), Turbulence characteristics and interaction between particles and fluid in particle-laden open channel flows, *J. Hydraul. Eng.*, 130(10), 988–1000, doi:10.1061/(ASCE)0733-9429 (2004)130:10(988).

Nezu, I., and H. Nakagawa (1993), *Turbulence in Open-Channel Flows*, 281 pp., A. A. Balkema, Rotterdam, Netherlands.

Nino, Y., M. Garcia, and L. Ayala (1994), Gravel saltation: 1. Experiments, *Water Resour. Res.*, 30(6), 1907–1914, doi:10.1029/94WR00533.

Nino, Y., F. Lopez, and M. Garcia (2003), Threshold for particle entrainment into suspension, *Sedimentology*, 50(2), 247–263, doi:10.1046/j.1365-3091.2003.00551.x.

Ninto, Y., and M. H. Garcia (1996), Experiments on particle-turbulence interactions in the near-wall region of an open channel flow: Implications for sediment transport, *J. Fluid Mech.*, 326, 285–319, doi:10.1017/ S0022112096008324.

O'Connor, J. E. (1993), *Hydrology, Hydraulics, and Geomorphology of the Bonneville Flood*, Geol. Soc. of Am., Boulder, Colo.

Parker, G. (1978), Self-formed straight rivers with equilibrium banks and mobile bed. Part 1. The sand-silt river, *J. Fluid Mech.*, 89, 109–125, doi:10.1017/S0022112078002499.

Parker, G. (1991), Selective sorting and abrasion of river gravel. Part II: Applications, *J. Hydraul. Eng.*, 117(2), 150–171, doi:10.1061/(ASCE) 0733-9429(1991)117:2(150).

Rouse, H. R. (1937), Modern conceptions of the mechanics of turbulence, *Trans. Am. Soc. Civ. Eng.*, 102, 463–543.

Schmeeckle, M. W., J. M. Nelson, J. Pitlick, and J. P. Bennet (2001), Interparticle collision of natural sediment grains in water, *Water Resour. Res.*, 37(9), 2377–2391, doi:10.1029/2001WR000531.

Seidl, M. A., and W. E. Dietrich (1992), The problem of channel erosion into bedrock, *Catena Suppl.*, 23, 101–124.

Seidl, M. A., W. E. Dietrich, and J. W. Kirchner (1994), Longitudinal profile development into bedrock: An analysis of Hawaiian channels, *J. Geol.*, 102, 457–474.

Sekine, M., and H. Kikkawa (1992), Mechanics of saltating grains. Part II, *J. Hydraul. Eng.*, 118(4), 536–558, doi:10.1061/(ASCE)0733-9429 (1992)118:4(536).

Shields, A. (1936), Anwendung der Aehnlichkeitsmechanik und der Turbulenzforschung auf die Geschiebebewegung, *Mitt. Preuss. Versuchsanst. Wasserbau Schiffbau*, 26, 26.

Sklar, L. S. (2003), The influence of sediment supply, grain size, and rock strength on rates of river incision into bedrock, Ph.D. thesis, 342 pp., Univ. of California, Berkeley, Calif.

Sklar, L. S., and W. E. Dietrich (2001), Sediment and rock strength controls on river incision into bedrock, *Geology*, 29(12), 1087–1090, doi:10.1130/0091-7613(2001)029<1087:SARSCO>2.0.CO;2.

Sklar, L. S., and W. E. Dietrich (2004), A mechanistic model for river incision into bedrock by saltating bed load, *Water Resour. Res.*, 40, W06301, doi:10.1029/2003WR002496.

Sklar, L. S., and W. E. Dietrich (2006), The role of sediment in controlling steady-state bedrock channel slope: Implications of the saltation-abrasion incision model, *Geomorphology*, 82(1–2), 58–83, doi:10.1016/ j.geomorph.2005.08.019.

Sklar, L. S., W. E. Dietrich, and A. D. Howard (1996), The influence of sediment supply on river incision into bedrock: A theoretical investigation, *Eos Trans. AGU*, 77(46), Fall Meet. Suppl., Abstract H32A–12.

Slingerland, R., S. D. Willett, and H. L. Hennessey (1997), A new fluvial bedrock incision model based on the work-energy principle, *Eos Trans. AGU*, 78(46), Fall Meet. Suppl., Abstract H42F–12.

Smith, J. D., and S. R. McLean (1977), Spatially averaged flow over a wavy surface, *J. Geophys. Res.*, *82*(12), 1735–1746, doi:10.1029/JC082i012p01735.

Sumer, B. M., and R. Deigaard (1981), Particle motions near the bottom in turbulent-flow in an open channel. Part 2, *J. Fluid Mech.*, *109*, 311–337, doi:10.1017/S0022112081001092.

Tinkler, K. J. (1997), Rockbed wear at a flow convergence zone in Fifteen Mile Creek, Niagara Peninsula, Ontario, *J. Geol.*, *105*, 263–274.

Tucker, G. E., and R. L. Slingerland (1994), Erosional dynamics, flexural isostasy, and long-lived escarpments: A numerical modeling study, *J. Geophys. Res.*, *99*, 12,229–12,243, doi:10.1029/94JB00320.

Turowski, J. M., D. Lague, and N. Hovius (2007), Cover effect in bedrock abrasion: A new derivation and its implications for the modeling of bedrock channel morphology, *J. Geophys. Res.*, *112*, F04006, doi:10.1029/2006JF000697.

Turowski, J. M., N. Hovius, H. Meng-Long, D. Lague, and C. Men-Chiang (2008), Distribution of erosion across bedrock channels, *Earth Surf. Processes Landforms*, *33*, 353–362, doi:10.1002/esp.1559.

Vanoni, V. A. (1946), Transportation of suspended sediment by water, *Trans. Am. Soc. Civ. Eng.*, *111*, 67–102.

van Rijn, L. C. (1984), Sediment transport: Part 2. Suspended-load transport, *J. Hydraul. Eng.*, *110*(11), 1613–1641.

Whipple, K. X. (2004), Bedrock rivers and the geomorphology of active orogens, *Annu. Rev. Earth Planet. Sci.*, *32*, 151–185, doi:10.1146/annurev.earth.32.101802.120356.

Whipple, K. X., and G. E. Tucker (1999), Dynamics of the stream-power river incision model: Implications for height limits of mountain ranges, landscape response timescales, and research needs, *J. Geophys. Res.*, *104*(B8), 17,661–17,674, doi:10.1029/1999JB900120.

Whipple, K. X., G. S. Hancock, and R. S. Anderson (2000), River incision into bedrock: Mechanics and relative efficacy of plucking, abrasion, and cavitation, *Geol. Soc. Am. Bull.*, *112*(3), 490–503, doi:10.1130/0016-7606(2000)112<0490:RIIBMA>2.3.CO;2.

Wiberg, P. L., and J. D. Smith (1985), A theoretical-model for saltating grains in water, *J. Geophys. Res.*, *90*, 7341–7354, doi:10.1029/JC090iC04p07341.

Wilcock, P. R., and J. C. Crowe (2003), Surface-based transport model for mixed-size sediment, *J. Hydraul. Eng.*, *129*(2), 120–128, doi:10.1061/(ASCE)0733-9429(2003)129:2 (120).

Wilcock, P. R., S. T. Kenworthy, and J. C. Crowe (2001), Experimental study of the transport of mixed sand and gravel, *Water Resour. Res.*, *37*(12), 3349–3358, doi:10.1029/2001WR000683.

Wobus, C. W., B. T. Crosby, and K. X. Whipple (2006), Hanging valleys in fluvial systems: Controls on occurrence and implications for landscape evolution, *J. Geophys. Res.*, *111*, F02017, doi:10.1029/2005JF000406.

Wren, D. G., S. J. Bennet, B. D. Barkdoll, and R. A. Kuhnle (2004), Distribution of velocity, turbulence, and suspended sediment over low-relief antidunes, *J. Hydraul. Res.*, *43*(1), 3–11.

Wright, S., and G. Parker (2004), Flow resistance and suspended load in sand-bed rivers: Simplified stratification model, *J. Hydraul. Eng.*, *130*(8), 796–805, doi:10.1061/(ASCE)0733-9429(2004)130:8(796).

Yager, E. M., J. W. Kirchner, and W. E. Dietrich (2007), Calculating bed load transport in steep boulder bed channels, *Water Resour. Res.*, *43*, W07418, doi:10.1029/2006WR005432.

_____

W. E. Dietrich and M. P. Lamb, Department of Earth and Planetary Science, University of California, 307 McCone Hall, Berkeley, CA 94720, USA. (mpl@gps.caltech.edu)

L. S. Sklar, Department of Geosciences, San Francisco State University, 509 Thornton Hall, 1600 Holloway Avenue, San Francisco, CA 94132, USA.